THE PHOSPHORYLATION OF PALLADIN AND THE EFFECT ON ITS INTERACTION WITH ACTIN BINDING, BUNDLING, AND POLYMERIZATION

A Thesis by

Joseph Gerard Brungardt

B.S., Benedictine College, Atchison, KS 2011

Submitted to the Department of Chemistry
and the faculty of Graduate School of
Wichita State University
in partial fulfillment of
the requirements for the degree of
Masters of Science

May 2013

THE PHOSPHORYLATION OF PALLADIN AND THE EFFECT ON ITS INTERACTION WITH ACTIN BINDING, BUNDLING, AND POLYMERIZATION

The following faculty members have examined the final copy of this thesis for form and content, and recommended that it be accepted in partial fulfillment of the requirement for the degree of Master of Science with a major in Chemistry.

Moriah R. Beck, Advisor and Chair

David M. Eichhorn, Committee member

James G. Bann, Committee member

Kandatege Wimalasena, Committee member

William J. Hendry III, Committee member

DEDICATION

To the two key educators in my life; Cassandra Brungardt and Dr. Aileen Beard

Even to your old age I am he,
even when your hair is gray I will carry you;
I have done this, and I will lift you up,
I will carry you to safety.

ACKNOWLEDGEMENTS

First and foremost I would like to thank my advisor, Dr. Moriah Beck, for her guidance and support during my time at Wichita State. Also, thank you to Ritu Gurung for being such a great friend and for taking the time to educate me on Nepalese culture. I must also mention two undergraduates in our lab that took on their projects with zeal and contributed so much to aiding me in lab; resident old guy Ty Dille and pseudo graduate student Erik Wong, best of luck in future endeavors. Thanks to my big brother in the department, Kiran Andra, who made it abundantly clear that you usually just have to try things out. Many thanks to the Bann Lab, Wimalasena Lab, and Dr. Bill Hendry who helped in what many ways they could. Financial support came from COBRE (8P20GM103420), KINBRE (P20RR016475), and the Flossie West Memorial Foundation. I would also like to thank the ladies in the office who get the dirty work done day-to-day, Debbie Mitchum and Laurie Reese. For my Excel tech support I must acknowledge Josh Beckman, the only guy to think a 30 MB spreadsheet is cool. Finally, thank you to my parents and family who love me without end.

ABSTRACT

Metastatic cell motility, namely breast cancer, has been shown to be regulated in part by the protein palladin. Palladin is a recently described actin binding and bundling protein whose expression level is related to metastatic cancer cell motility. Palladin plays a role in the regulation of actin, a highly abundant protein within a cell, which acts as a cell's skeleton. Actin is also the structural basis of invasive cellular structures known as invadopodia, which cross the extracellular matrix and allow cells to invade surrounding tissue structures. Palladin has been shown to regulate actin bundles within these invasive structures. Further studies have shown that Akt1, a prominent and highly studied protein kinase, phosphorylates palladin at a linker region between its immunoglobulin domains that are critical for actin bundling. Our work builds upon initial cell-based assays which show that normal cell function is altered when phosphorylation of palladin is misregulated. We utilized biochemical assays to quantify how phosphorylation of palladin affects the structure and function of actin to further understand both of their roles in cancer cell motility.

TABLE OF CONTENTS

TABLE OF CONTENTS (continued)

TABLE OF CONTENTS (continued)

LIST OF TABLES

LIST OF FIGURES

LIST OF FIGURES (continued)

LIST OF ABBREVIATIONS

ADP	Adenosine Diphosphate
ATP	Adenosine Triphosphate
BAL	Benzamidine, Antipain, Leupeptin
Ca^{2+}	Calcium ion with 2+ charge
DNA	Deoxyribonucleic Acid
DTT	Dithiothreitol
EDTA	Ethylenediaminetetraacetic acid
F-Actin	Filamentous Actin
FPLC	Fast Protein Liquid Chromatography
G-Actin	Globular Actin
GE	General Electric
HEPES	4-(2-hydroxyethyl)-1-piperazineethanesulfonic acid
Ig34 P	Palladin Immunoglobulin Domain 34 Phosphomimetic
Ig3L P	Palladin Immunoglobulin Domain 3L Phosphomimetic
kDa	Kilodaltons
Mg^{2+}	Magnesium ion with 2+ charge
PDB	Protein Data Bank
pH	pH = log10(1/[H+])
pI	Isoelectric point
Pi	Phosphate
PMSF	Phenylmethylsulfonyl Fluoride
SDS-PAGE	Sodium dodecyl sulfate polyacrylamide gel electrophoresis

LIST OF ABBREVIATIONS (continued)

SEM	Standard Error of the Mean
TEV	Tobacco Etch Virus
UV/VIS	Ultra Violet/Visible

1. INTRODUCTION

1.1 Actin

Actin is a highly abundant protein which exists within most eukaryotic cells and serves many functions as a means of transportation, structural support, and signaling [1]. First described by Bruno Straub in 1942, actin was originally observed as the major component of muscle and it was discovered, by the same group, that it existed in monomeric or globular form in the absence of salt and as a polymer or filament in the presence of salt [2]. It is this dual form that actin takes on which gives it both a dynamic role in eukaryotic cells and has allowed it to remain so highly conserved throughout living organisms. Actin can form single filaments and these single filaments can then be bundled together to make larger structures. These bundled structures have been found to play an important role in the ability of cancer cells to move and are the structures that are of most interest here.

1.1.1 Structure of Actin

Actin exists in both globular and filamentous forms, or G-actin and F-actin. G-actin is comprised of 374 amino acid residues in a single polypeptide chain and has a mass of 41,785, or 42,300 when accounting for bound ATP and Ca^{2+} [3]. In the globular or filamentous form, actin contains either an adenosine triphosphate or adenosine diphosphate and either a magnesium or calcium divalent cation [4, 5]. G-actin is comprised of two major domains which are each then divided into two subdomains [6]. This structure is shown in Figure 1.1. The small domain, on the right, is divided into subdomains 1 and 2, while the large domain, on the left, is divided into subdomains 3 and 4. The G form of actin contains a single binding site for the nucleotide and a single high affinity site for a cation. This nucleotide binding site is between subdomains 2 and 4

in the cleft which is above the groove running through the center of the large and small domain. The binding site for the divalent cation is just below this cleft. There are also a number of low affinity sites where these cations can associate to and in turn affect the polymerization dynamics of the G to F form [6]. At physiological pH, the isoelectric point of actin is 4.8, thus carrying a net negative charge overall [3, 7]. These charge characteristics of the protein play an important role in its polymerization from G-actin to F-actin. Actin has an end designated the minus end (the slow end or pointed end) and the plus end (the fast end or barbed end) [8]. In Figure 1.1 the minus end is shown between subdomains 2 and 4 while the plus end is between subdomains 1 and 3. It is important to note that the plus end of actin polymerizes faster than the minus end. The quaternary structure of actin, the filamentous form, can exist as an independent structure, but more often it makes up a larger aggregated structure, either wrapped around itself, branched, cross-linked, or bundled to make up larger structures within a cell.

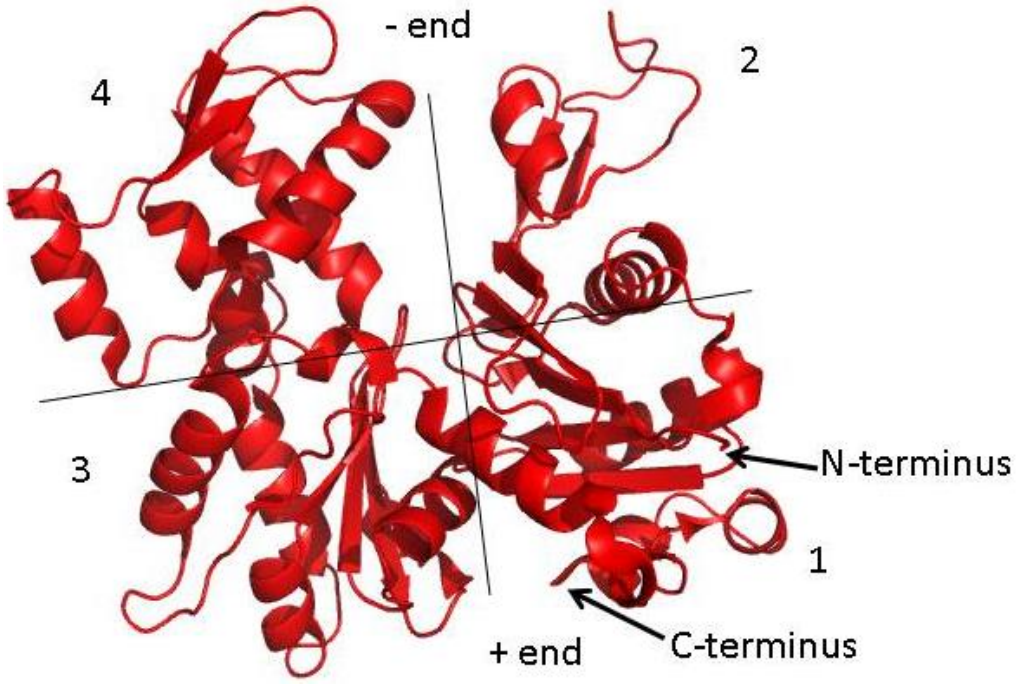

Figure 1.1 The X-Ray Crystal Structure of G-Actin, PDB ID: 1ATN [6, 9]. Subdomains 1, 2, 3, and 4 are designated as are the – (pointed) and + (barbed) ends. The ATP/ADP binding cleft is between subdomains 2 and 4.

The structure of the filamentous form is often depicted in cartoon representations as clamshell-like G-actin strung together in an ADP-bound state. This structure is depicted in Figure 1.2. The filamentous structure has remained unsolved directly by X-ray crystallography due to its size but a low resolution reconstruction to create an accurate model was first done by Holmes in 1990 from the structure of G-actin and incomplete X-ray data [10]. This structure showed F-actin as a double helix, with two filaments wrapping around each other. More recently, the structure was solved using advances in electron cryomicroscopy to 6.6 angstrom resolution and modeling simulations with G-actin [11].

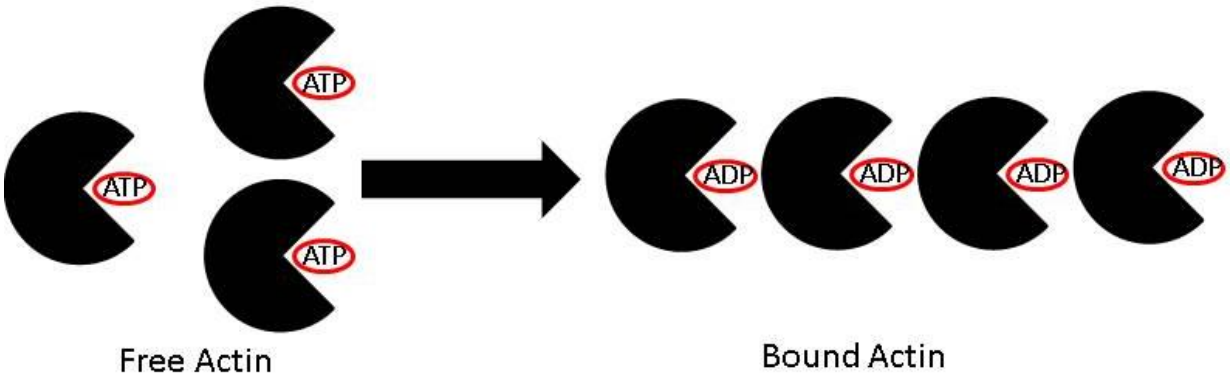

Figure 1.2 The Polymerization of Actin From the Globular to Filamentous State. Monomeric actin nucleates before polymerization to the filamentous form and subsequently ATP is hydrolyzed to ADP.

Actin filaments can form a number of larger structures and networks within a cell. These can be crosslinked filaments, where the filaments are bound together perpendicularly by an actin-binding protein. There can also be branching, where a new filament is polymerized away from a primary filament. Capping occurs when a protein stops the polymerization of a filament. Finally, there is bundling, where filaments are bound parallel to one another. These structures are depicted in Figure 1.3.

1.1.2 Function of Actin

The dynamic relationship between the globular and filamentous forms of actin revolves around its binding of ATP or ADP, and the ionic strength of the environment. In the monomeric state, actin binds ATP and upon polymerization, eventually hydrolyzes this ATP to ADP, unless it is at the plus end [12]. To begin polymerization, three actin monomers must aggregate or nucleate to form the filament. When in the monomeric state, K^+ and Mg^{2+} can be added to induce polymerization. This is thought to occur because of a reduction in net negative charge on actin, about 15 at neutral pH, and thus a reduction in repulsion between actin monomers [4, 8, 13]. It is important to note that ATP-actin polymerizes faster than ADP-actin and that ATP-actin depolymerizes from a filament more slowly than ADP-actin [13]. This process of actin polymerization and depolymerization is called treadmilling and is regulated through proteins that nucleate monomers, cap filaments, aid polymerization, help depolymerization, or control ATP/ADP exchange which in turn regulates the polymerization and depolymerization kinetics. As noted previously, actin is able to polymerize in either ATP or ADP-bound states [14]. This then raises the question of what role either nucleotide plays in the polymerization of actin. Since the hydrolysis of ATP is not necessary for polymerization, its role as an energetic molecule is defunct. Both random mechanisms and controlled mechanisms have been proposed for the actual hydrolysis of ATP after polymerization but turnover does not happen immediately [12, 15-17]. In any case, monomers in the ATP-bound state have a greater affinity for one another than those in the ADP-bound state. This is due in part to a conformational change in the nucleotide binding cleft, which favors a closed conformation in ATP or ADP-Pi states and an open conformation in the ADP-bound state [18].

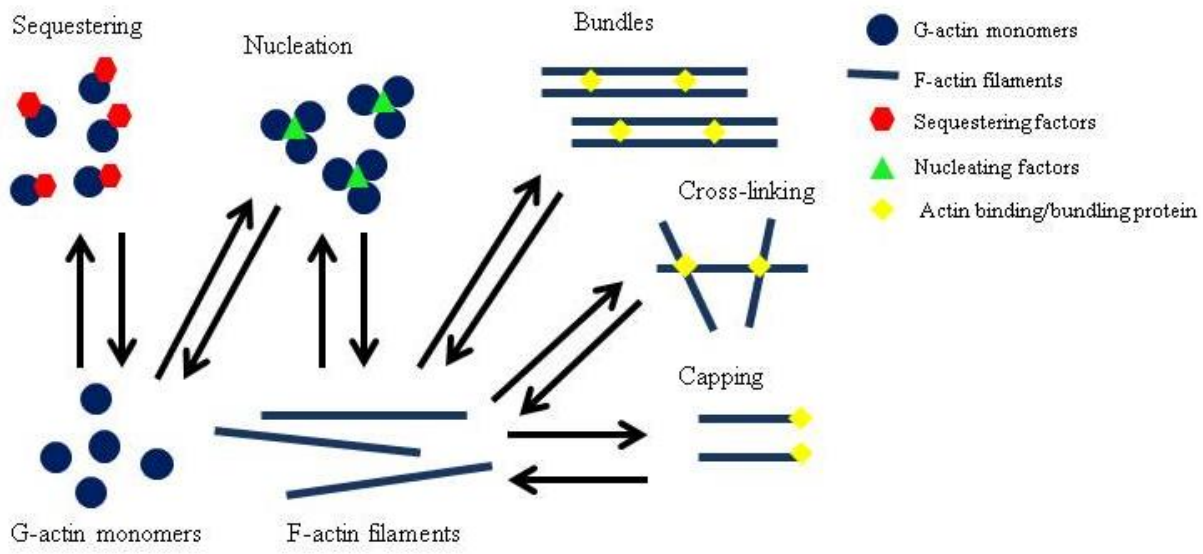

Figure 1.3 The Possible Structures of Actin Networks [19]. Filamentous actin can be bound together in parallel to form bundles or bound orthogonally to form cross-linked structures.

1.1.3 Cellular Role of Actin

Actin takes on a number of roles within the cell and within larger eukaryotic structures. It is a major component of muscle cells and the cell cytoskeleton, takes part in cytokinesis, gives both rigid and flexible cell support, creates cell protrusions which aid in locomotion, organizing signaling molecules, and more [20-23]. These various functions within the cell are controlled by a number of actin-binding proteins, of which there are over 150 [24]. With this amount of peripheral proteins involved in regulation of actin polymerization, the importance of polymerization cannot be overlooked and it is easy to see how misregulation of one piece affects so many other processes within the cell. The cell structures, which actin makes up a large part of, are distinct morphological landmarks within healthy and cancerous cells.

The cellular structures that actin is involved with and which interest the work presented here primarily include both podosomes and invadopodia. These two structures are very similar in shape and function but differ in that invadopodia cross the extracellular matrix [25]. Podosomal formation in cells is often found in healthy cells that must move such as macrophages, dendrites,

and osteoclasts as part of their normal function [26-28]. Invadopodia, on the other hand, have been defined in early years as differing because of their ability to degrade the extracellular matrix. More recently this has been called into question by studies showing podosomes which can cause degradation in healthy or normal cell function [29]. Invadopodia present as random finger-like protrusions, whereas podosomes form a more ring-like association; but structure and function of the two units remains very similar [30]. The debate as to whether or not these structures are the same thing but act in different ways remains, but structurally speaking invadopodia have a greater 'reach' through the extracellular matrix. With such a pivotal role in cell motility though, understanding how both podosomes and invadopodia function is equally important. Representations of these components with regards to cells and an extracellular matrix are shown in Figure 1.4 [31].

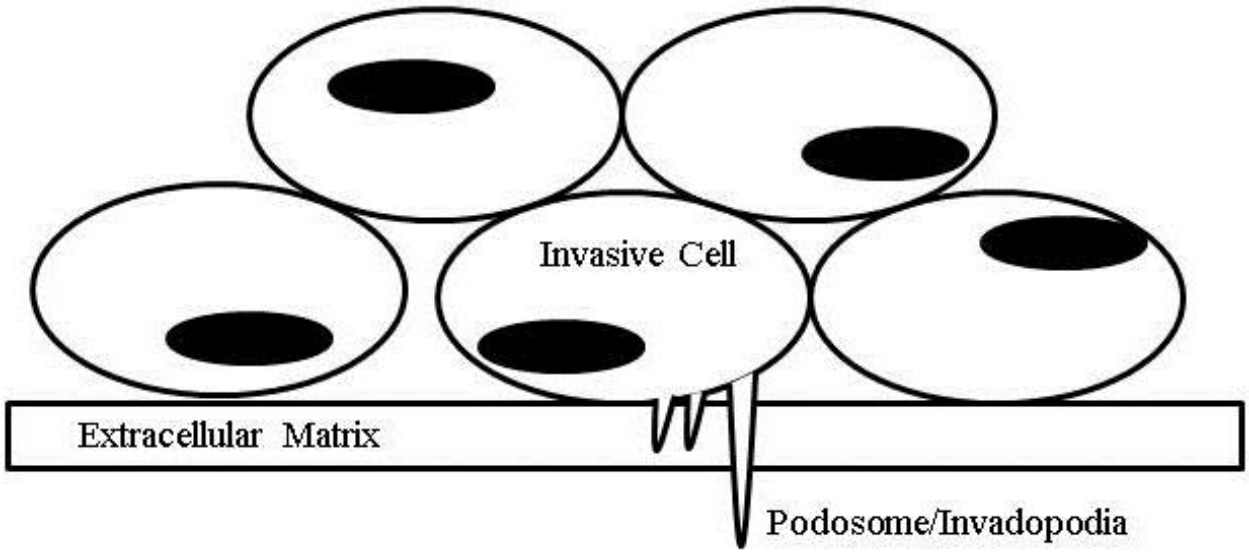

Figure 1.4 Invasive Cell Podosomes. The podosomes or invadapodia break through the extracellular matrix before metastasis to other organ or tissue systems.

The more intricate differences of podosomes and invadapodia are contained in a discussion of the extra- and intracellular molecular processes of each. The role of actin in both is an intracellular process, one which involves giving the structures their shape, strength, and

elasticity [30]. Actin within the structures is depicted in Figure 1.5. These structures are about 1μm long and packed with actin bundles for stability [32]. These bundles of actin in the core is a feature that makes these two structures distinct from others which contact the extracellular matrix [33]. Structurally, the filamentous actin forms stress fibers in normal motile cells while in invasive cells the packing of actin is more dense in the invadopodia and is packed in a criss-cross fashion [32].

The role of invadopodia in cancer can be described by its projection into the extracellular matrix, degradation of this structure, and eventually allowing a cell to pass through this membrane [25]. The extracellular matrix is a conglomerate of protein, proteoglycans, and other macromolecules excreted by tissue cells [34]. It not only serves to separate cells but also plays some role in the regulation of cell movement and cell-cell signaling. When a primary cancer tumor is able to break through the extracellular matrix, it becomes metastatic and can localize to another area of the body, beginning a tumor growth separate from the primary tumor. The regulation of actin, which in turn affects podosome and invadopodia formation in cancers, is therefore important to understand and is the focus of the work here.

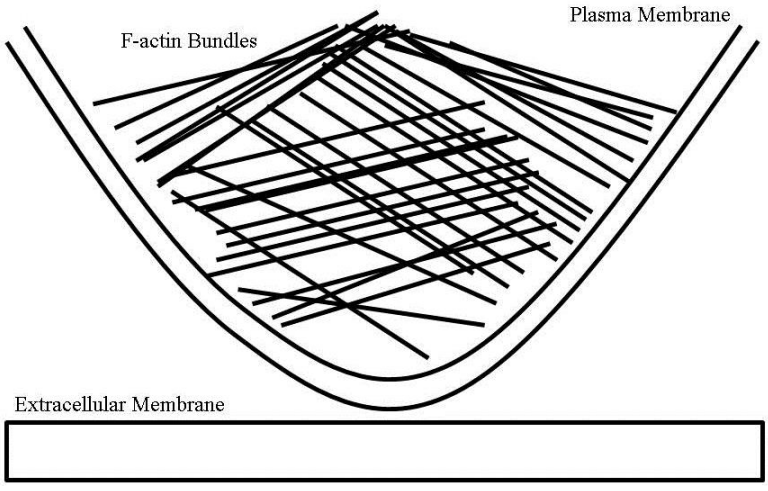

Figure 1.5 Actin in the Podosome. Actin is crosslinked or bundled to form the structural basis of the invasive podosome or invadopodia structure.

1.2 Palladin

Palladin is an intracellular protein that is involved in regulation of cytoskeletal cell functions and motile structures. Palladin was a protein first described in 2000 by Otey and was shown to be associated with both actin and α-actinin and in turn the structures these proteins comprise [35]. Multiple studies have shown the range of structures necessary for motility that palladin is associated with such as dorsal ruffles, podosomes, and developing cells [36, 37]. As an actin binding protein, palladin also bundles actin, and therefore is not simply acting as a regulator but also a scaffold through its binding of other proteins [38]. As discussed previously, formation of the actin bundle structure is important in the mechanisms of cancer metastasis so it is of interest to us to study palladin and its specific biochemical interaction with actin.

1.2.1 Structure of Palladin

Palladin was first described as a 90 and 92 kDa doublet [35]. Since then palladin has been observed expressed in humans as seven different isoforms, shown in Figure 1.6, which localize to various cell types [39-41]. The 200 kDa isoform is found in heart tissue, the 140 kDa isoform is found in epithelial tissue, and the 92 kDa isoform is found expressed in all types of tissue. The other four isoforms at 122 kDa, 128 kDa, 59 kDa, and 43 kDa have been detected with their apparent molecular weight being undetermined [41]. The expression of the different sizes of isoforms likely is rooted in tissue specific regulation considering the localization of different isoforms to different tissues.

Immunoglobulin domains, or Ig domains, are a defining trait of palladin, whose largest isoform contains five such domains and whose 92 kDa isoform, which is most highly expressed, contains three [39, 42]. The two N-terminal Ig domains are separated from the three C-terminal Ig domains by two polyproline-rich regions which is found in other actin-associated proteins like

vinculin and vasodilator stimulated phosphoprotein [35]. The C-terminal Ig domains are called Ig C2 domains, which have previously been found in actin cytoskeletal proteins like C protein, H protein, M protein, titin, and myotilin [43-47]. The structures of the third and fourth Ig domains of palladin, Ig3 and Ig4, are shown in figure 1.7, in red and blue, respectively. These Ig C2 domains are about 100 amino acids in length, about 12 kDa, and contain between 8 or 9 beta strands in a sandwiched beta sheet fold [38]. With such a structural similarity to other proteins involved in regulation of cell morphology, a parallel can be drawn to the role of palladin as a cytoskeletal regulator.

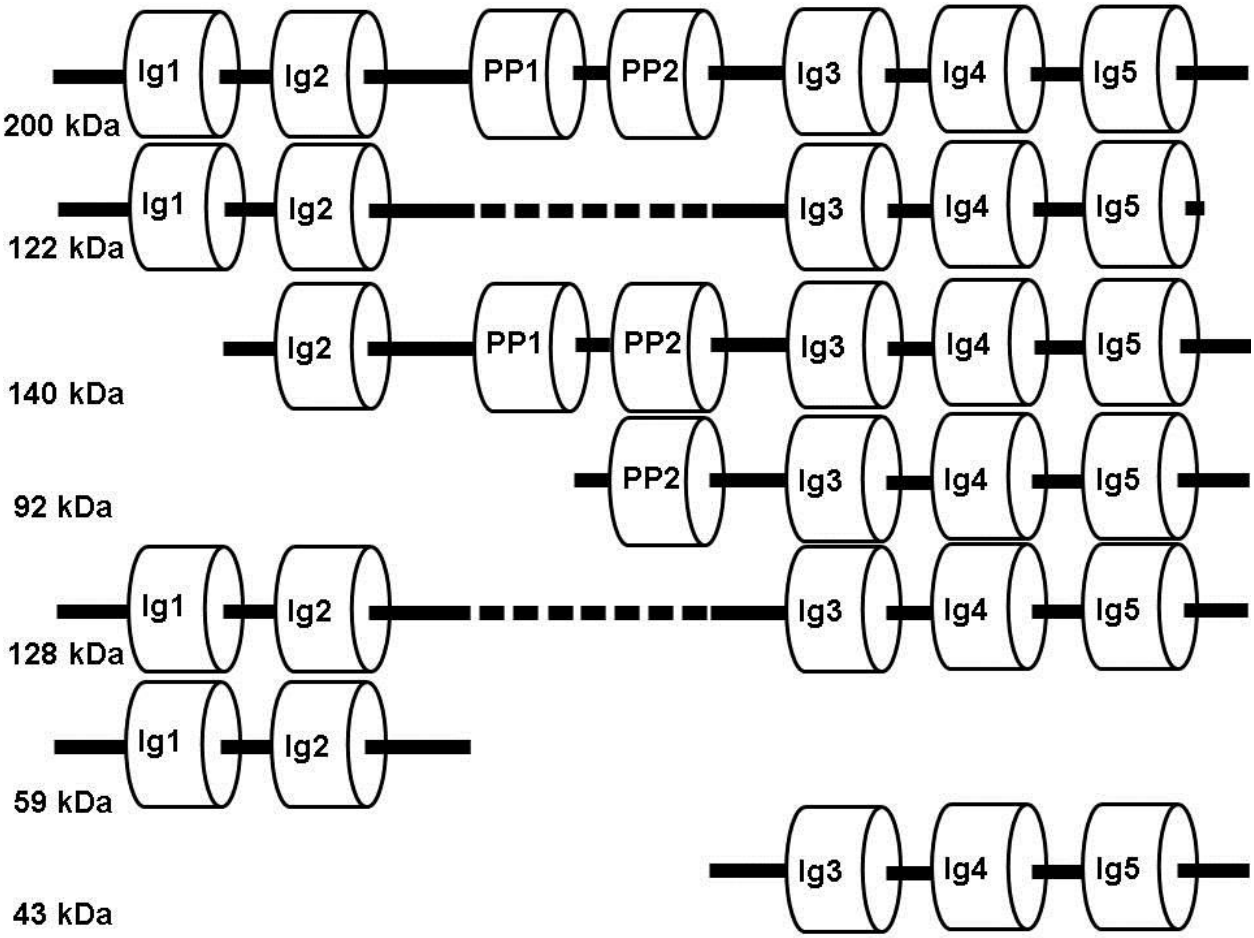

Figure 1.6 The Isoforms of Palladin. Isoforms 1 through 7, from top to bottom, with apparent weight displayed when protein is observed and theoretical weight displayed when not observed.

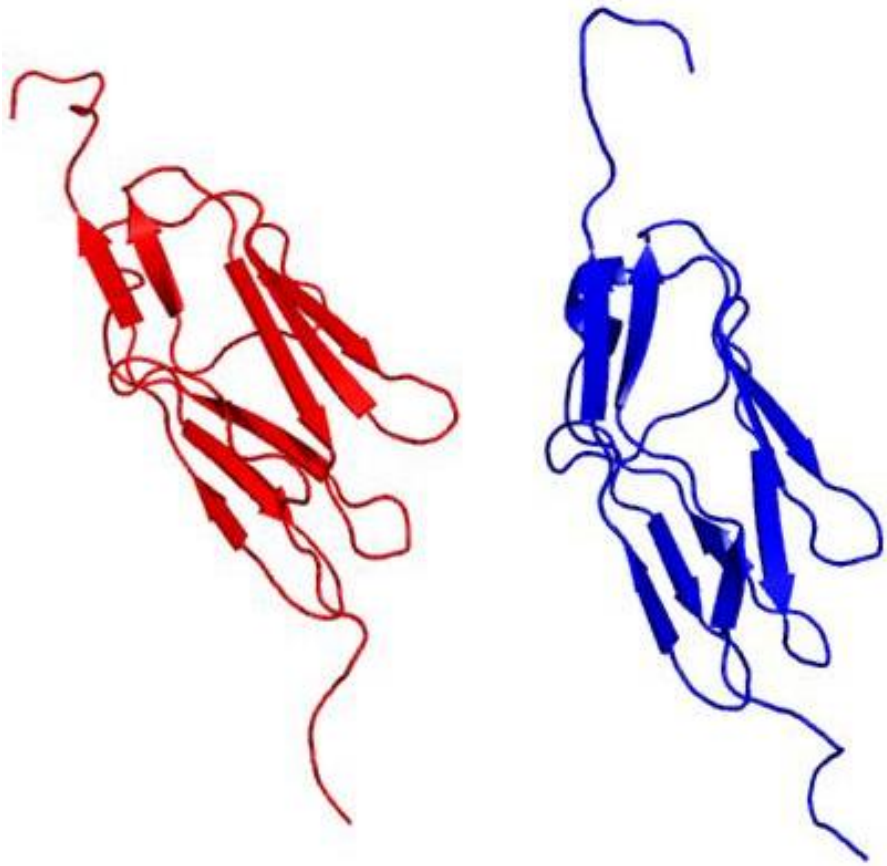

Figure 1.7 Ig3 and Ig4 NMR Solution Structures PDB ID: 2DM2 & 2DM3 [9]. Ig3 (red) and Ig4 (blue) domains of palladin showing sandwiched beta sheet fold.

1.2.2 Function of Palladin

While the function of the two N-terminal Ig domains remains unknown, the domains that we are interested in are the Ig3, Ig3L, and Ig34 domains, domains known to be necessary to bind or bundle actin filaments [38, 40]. Ig3 refers to the third Ig domain alone. Ig3L refers to the Ig3 domain with the linker region at the C terminus. Ig34 refers to the Ig3 domain expressed with the linker region and Ig4 domains in tandem. The Ig4 and Ig5 domains have been shown to bind to ezrin, a protein associated with actin scaffolding [42]. Other binding partners include MRTF, a transcription factor, Eps8, which interacts with kinases and growth factors, and vasodilator stimulated phosphoprotein, a protein that also regulates actin [36, 48, 49]. These interactions and how it affects the network of intracellular signaling have yet to be fully understood, but the

specific role of palladin as a player in the movement and growth of cells can be immediately surmised.

The Ig domain proteins that have structures and functions similar to palladin are myosin-binding protein C, titin, myopalladin, and myotilin. These proteins have similar structures and are found in the cytoplasm, unlike other immunoglobulin domain proteins which are usually found associated with the plasma membrane [40]. Myosin-binding protein C, which contains seven of these Ig domains, binds to myosin, titin, and actin. While the Ig C1 and C2 domains bind myosin along with the C8-C10 domains, the titin binding site is at C9-C10, and the C5 and C8 domains are shown to bind to each other, which suggests dimerization capabilities [50-52]. The actin-binding and bundling region of myosin-binding protein C is found on the N-terminus, and the domains from C0 to C4 have been shown to have actin affinity [53]. Titin acts as a myosin and actin binding protein, but binds actin in its PEVK domain (Pro-Glu-Val-Lys), not one of its Ig domains [54]. Titin has similar functions to palladin, such as scaffolding multiple proteins, signaling, and aiding in cell structure. The Ig domains of titin remain difficult to study though as it is over 3 megadaltons in size and has 160 copies or more of the Ig domain when considering its multiple isoforms. Myopalladin is closely related to palladin in overall structure, containing five Ig domains but no proline rich region [55]. Studies have shown myopalladin necessary for structural regulation of muscle cells and involved in some cardiomyopathies [56]. Myotilin on the other hand contains only two Ig domains but is also found expressed in striated muscle cells like titin [47]. These Ig domains were shown to bind actin as well as bind each other as dimers. This dimerization allows for actin cross-linking, which could suggest a similar mechanism might be used by palladin and its Ig domains [57].

The function of palladin as an F-actin binding and bundling protein is of greatest interest to us and thus the C-terminal domains are those that we study. Initial studies showed Ig3 as the minimal domain necessary to bind F-actin [38]. Palladin was also shown to be an actin bundling protein, with Ig34 being the minimal domain necessary to fulfill this role. The Ig4 and Ig5 domains do not bind or bundle filamentous actin, but the addition of Ig4 to Ig3, separated by the linker region, was shown to increase binding affinity over that of Ig3 alone, with Ig3 binding actin at a Kd of ~70 μM and Ig34 having a Kd of ~10 μM. The results from these studies are reproduced in Figure 1.8. With previous studies showing that the linker region alone and the Ig4 domain alone are not capable of binding to filamentous actin, the increase in affinity and addition of these domains suggest that their presence increases the Ig3 affinity or Ig3 enhances their own affinity [38]. This enhancement of binding upon the addition of the linker region and Ig4 suggest that either the linker or Ig4 domain undergoes a conformational change when joined with Ig3 since Ig4 does not bind F-actin when expressed as a single domain. Other possible explanations for this are the dimerization of the Ig34 domain, where one Ig34 domain binds actin, and then dimerizes on itself to present an additional actin binding domain to another actin filament. Either conformational change or dimerization could explain the increase in affinity and bundling capabilities of Ig34.

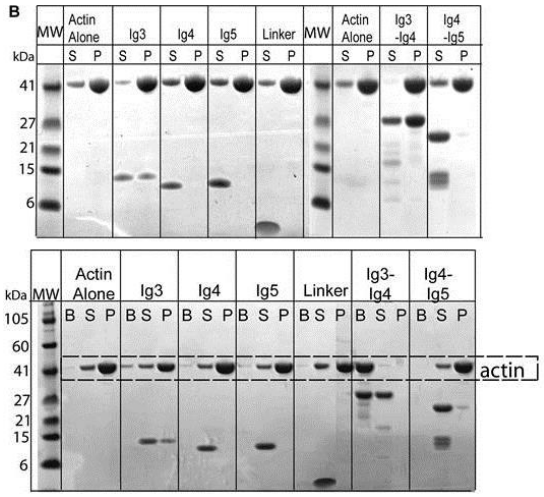

Figure 1.8 Initial Binding and Bundling Studies of Palladin. Previous work shows Ig3 as the minimal palladin domain necessary to bind actin and Ig34 as the minimal domain necessary to bundle actin [38].

An unusual feature of Ig3 is that no other single Ig domain has been found to bind actin on its own, as the Ig domains capable of binding actin are usually found in tandem repeats. It is important to note that there is no consensus actin-binding motif. Rather, multiple types of tertiary structures exist which are capable of binding G- and F-actin. A good example of this is filamin A that has two distinct domains which are both capable of binding actin, one comprised of alpha helices and the other consisting of immunoglobulin domains [58, 59]. Most actin binding protein domains are comprised of alpha helices, such as the proteins gelsolin, DNaseI, profilin, twinfilin, and the FH2 and WH2 alpha-helical domains [60, 61]. Palladin is a unique protein, in that it is in a minority of actin binding proteins with its Ig actin binding domain and that it has a single immunoglobulin domain, Ig3, capable of binding actin. Its unique structure and function, coupled with its role in cancer metastasis, are part of the cause for our interest in palladin.

1.2.3 Importance and Role of Palladin In the Cell

Palladin's function as a scaffolding protein can be drawn from all of these interactions with its binding partners, many of which are also involved in cytoskeletal regulation. Ezrin has

been shown to link the cytoskeleton of a cell with the plasma membrane [62]. Moreover, ezrin has a large role in the assembly and regulation of new and growing microvilli and human carcinomas [63]. MRTF, also called MKL1, is a transcription factor that is found in the nucleus and is regulated by the concentration of G-actin in the cytosol [64]. The interaction of MRTF with actin is part of a transcription and regulation model that describes it as playing a major role in signaling the nucleus in response to cytoskeletal changes as well as regulating muscle cell differentiation [65]. Eps8 stimulates Rac protein activation, which leads to a change in actin dynamics and enhanced motility [66]. Besides this function, Eps8 binds to other proteins like EGFR and actin [36, 67]. Vasodilator stimulated phosphoprotein, or VASP, is also heavily involved in motile cells, appearing in the leading edges of migrating cells, promoting actin polymerization, and capable of binding to both G and F-actin, while also stabilizing polymerized actin filaments [68]. Palladin's wide array of binding partners highlights its role as an actin scaffolding protein and regulator of actin dynamics within the cell.

Initial studies described palladin as necessary for normal cytoskeletal organization and formation of focal adhesions in both fibroblasts and neuronal cells, having a role in differentiating dendritic cells, taking part in wound-healing through myofibroblasts, and localizing to dorsal ruffles in motile cells [35, 36, 42, 69, 70]. These cell-based studies gave initial data on the function of palladin within the cell and later biochemical assays have determined specific interactions with other protein structures. The interaction of palladin and actin is highlighted throughout these studies. When palladin was initially discovered, its upregulation was observed when the growth of stress fibers and focal adhesions, critical structural components of the cell cytoskeleton, were stimulated [35]. This same study also showed decreased focal adhesions and stress fibers upon palladin knockdown. These first studies

were done with a cell model that is involved in developing embryos, but a later study with a neuronal cell model showed similar utilization of palladin when knockouts were performed on growing cells [69]. Palladin was found in growth cones of developing dendrites and outgrowth of immature dendrites failed when knockouts were performed. Possesing a role in growth of embryonic and neuronal cells, palladin is also found in the podosomes of maturing dendritic cells and invasive stomach cancer cells [42]. One study also found palladin to take a role in differentiation of myofibroblasts into smooth muscle cells while also colocalizing with actin [70]. Finally, an initial study showed palladin present in dorsal ruffles; actin rich structures that have a role in reorganization of the cell membrane before cell migration or signaling [36]. Knockdown of palladin in this study decreased dorsal ruffle formation and was also shown to increase podosome formation, localizing there as well. Through these studies done in the first six years after the discovery of palladin, a foundation for its function and importance as a cytoskeletal scaffolding protein has been laid, but many areas still remain unclear.

The role of palladin in metastatic cancer cell motility has been investigated in numerous studies. Specifically, recent studies showed palladin to be upregulated in metastatic breast cancer cells [71]. The expression levels of palladin within these highly invasive cells is much greater than in healthy cells and knocking down palladin reduces podosome formation, migration, and invasive motility [71]. Besides breast cancer, isoforms of palladin were observed in invasive pancreatic cancer [41]. More recently, a study showed poor clinical outcome in patients whose palladin expression was higher than patients whose palladin expression levels were low [72]. This correlation between palladin and poor outcomes, measured by prognosis or presence of local and distant metastases, was stronger than other clinical markers tested in that particular study. Finally, one recent study showed palladin expression enhances migration of cells as well

as induces invadopodia formation [73]. This particular study showed the invadopodia tunneling through extracellular matrix to allow other cells to invade. The upregulation of palladin has been strongly linked to metastatic cancer and has been shown to be a key player in cancerous cell motility through the regulation of the formation of invasive cell structures.

1.3 Akt1 and Protein Phosphorylation

While palladin upregulation has been correlated with invasive cell motility, the factors regulating palladin within healthy and cancerous cells is not well understood. While this remains to be determined, one way many proteins are regulated, besides gene regulation, is through post-translational modifications. These are additions to the primary structure of a protein, such as the addition of a sugar or phosphate, or the removal of some amino acids. After this change to the primary structure of a protein, post-translational modifications regulate function by changing secondary and tertiary structure, changing the chemical environment of the protein. One of the post-translational modifications of palladin is phosphorylation by Akt, also known as protein kinase B [74]. Phosphorylation of a protein is the addition of a phosphate group to an amino acid side chain, which in the case of palladin is a serine residue located in the linker region between the Ig3 and Ig4 domains at the recognition sequence RXRXX(S/T) which is RPRSRS in the linker region [74, 75]. The kinase family capable of doing this, Akt, has been shown to play a role in the PI3-K signaling pathway [76]. The phosphoinositide 3-kinase, PI3-K, signaling pathway is often deregulated in metastatic cancer [77].

The PI3-K pathway is activated by a number of possible events, but goes on to phosphorylate phosphatidylinositol 4,5-bisphosphate, PIP_2, into phosphatidylinositol (3,4,5)-trisphosphate, PIP_3. This product binds, among many other proteins, Akt at the cell membrane which in turn activates cell cycle entry, survival, and protein synthesis [78, 79]. Akt has three

isoforms in the family, Akt1 or PKBα, Akt2 or PKBβ, and Akt3 or PKBγ. Interestingly, Akt1 appears in some studies to inhibit cell invasion and motility in breast cancer cell models but increase tumor growth, whereas Akt2 has been shown recently to increase invasive activity [80, 81]. These events are depicted in Figure 1.9.

This difference in function between the Akt1 and Akt2 isoforms has been shown both through *in vitro* and *in vivo* studies, but the mechanism by which Akt1 and Akt2 selectively phosphorylating substrates is unknown [76]. Palladin is one such substrate of Akt, where Akt1 is capable of phosphorylating the serine in the linker region but Akt2 is not [74]. While Akt2 does not directly modify palladin, it is capable of upregulating it by increasing expression [75].

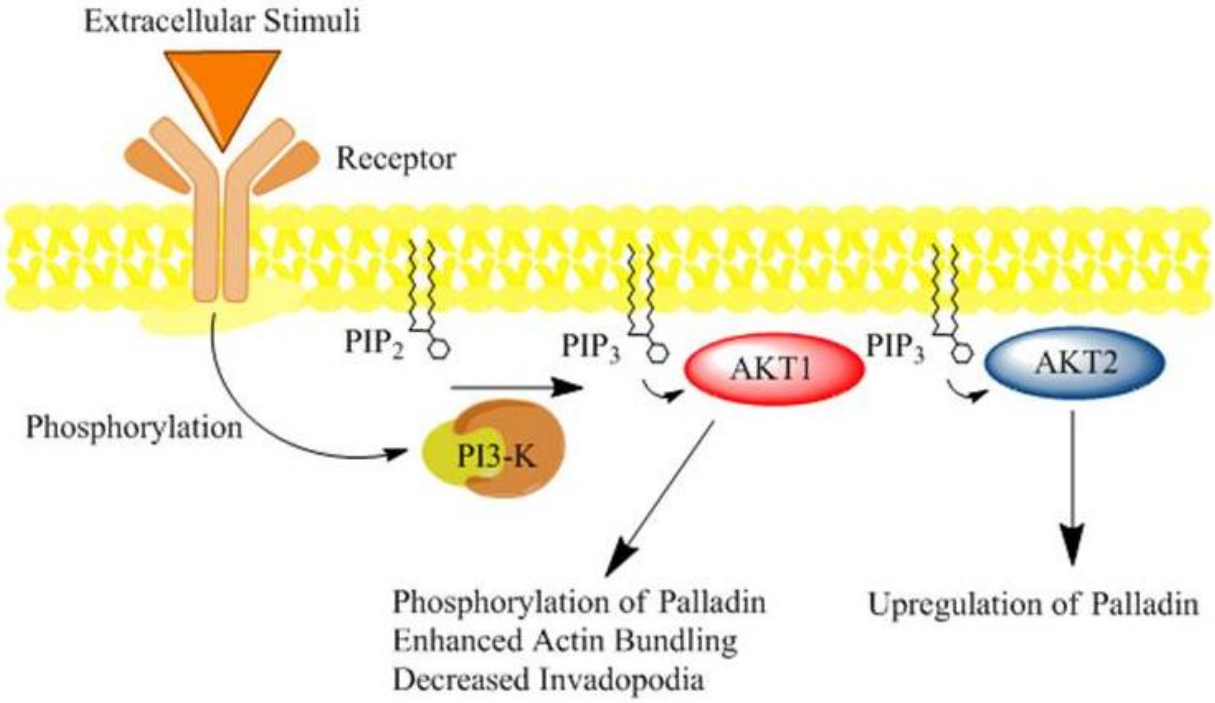

Figure 1.9 AKT1 Signaling In The Cell. Extracellular factors activate the PI3-K signaling pathway. PI3-K converts PIP_2 to PIP_3. PIP_3 activates Akt which affects palladin by phosphorylation or upregulation.

1.3.1 Role of Akt and Palladin in Cell Function

Chin and Toker recently undertook studies investigating the effects of palladin phosphorylation by Akt1 and Akt2 and its role in cell models [74, 75, 82]. Knockdown assays of palladin showed enhanced invasive cell migration. Their studies also showed that increased expression of Akt1 slows migration, and that palladin knockdown again increases cell invasion. They showed that the enhanced migration caused by knockdown of palladin could be slowed by reintroduction of a wild type palladin allele. However cells remained invasive when an allele with the serine 507 in the linker region mutated to alanine was introduced in palladin, blocking the ability of Akt1 to phosphorylate palladin [74]. Co-sedimentation assays performed with pure F-actin and crude cell lysates showed equal binding affinity but increased bundling capability by the wild type palladin. Finally, decreased invadopodia formation was equally observed with both wild type and mutant palladin. This first study on Akt1 and its interaction with palladin proposes that while palladin expression plays a crucial role in cell migration, its regulation by post-translational modification is also very important.

While palladin is not a substrate for phosphorylation by Akt2, this kinase still regulates its expression [75]. Upon inhibition of Akt2 using multiple inhibitors, expression levels of palladin decrease over time. Knockdown of Akt2 was shown to decrease palladin expression by more than half, while Akt1 knockdown had no effect. Palladin phosphomimetic mutants proved to be unaffected in their expression when the PI3-K pathway was inhibited when compared to wild type and alanine mutants. This study implies that the Akt family of kinases, proven to be key players in cancerous cell proliferation, have a role in the regulation of the expression levels of palladin.

When considering palladin in other cell motility studies, increased expression of palladin was accepted as a cause for increase in cell motility and migration [71, 73]. Chin and Toker's work though suggests that this does not provide a complete explanation and that the phosphorylation of palladin and the Akt1/Akt2 relationship probably influences palladin's role in invasion. Indeed, this has been shown in other actin binding proteins phosphorylated by Akt that play a role in cell motility and invasion within breast cancer cell lines.

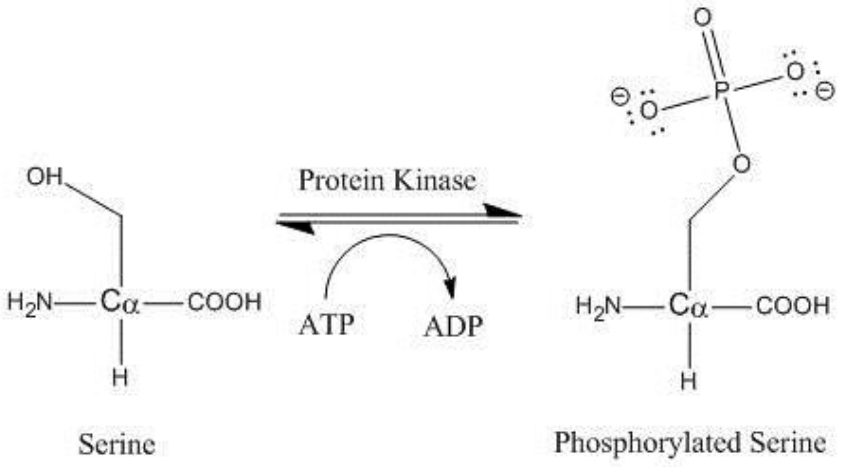

Figure 1.10 The Phosphorylation of Serine by a Protein Kinase

1.3.2 The Effect of Phosphorylation on Palladin

The phosphorylation of palladin by Akt1 occurs at a serine within the linker region between the Ig3 and Ig4 domains, the domains critical for actin binding and bundling [74]. Akt1 recognizes the phosphorylation motif (RXRXXS/T) at this region whose specific amino acids are RPRSR**S**R. This event is depicted by the general reaction with serine in Figure 1.10. To mimic this in our own work, we used a glutamic acid mutation at this serine position. Phosphomimetic mutations have been widely used in both *in vivo* and *in vitro* biochemical studies [83-85]. The most obvious difference after this mutation, which is depicted in Figure 1.11, is the presence of the negative charge, which lies between the positive charges of the arginine residues. This

negative charge of the glutamic acid simulates the presence of a phosphate group in a reproducible and controlled manner. This phosphomimetic will be referred to throughout the text as Ig3L P or Ig34 P, the phosphomimetics of the Ig3L construct or the Ig34 construct.

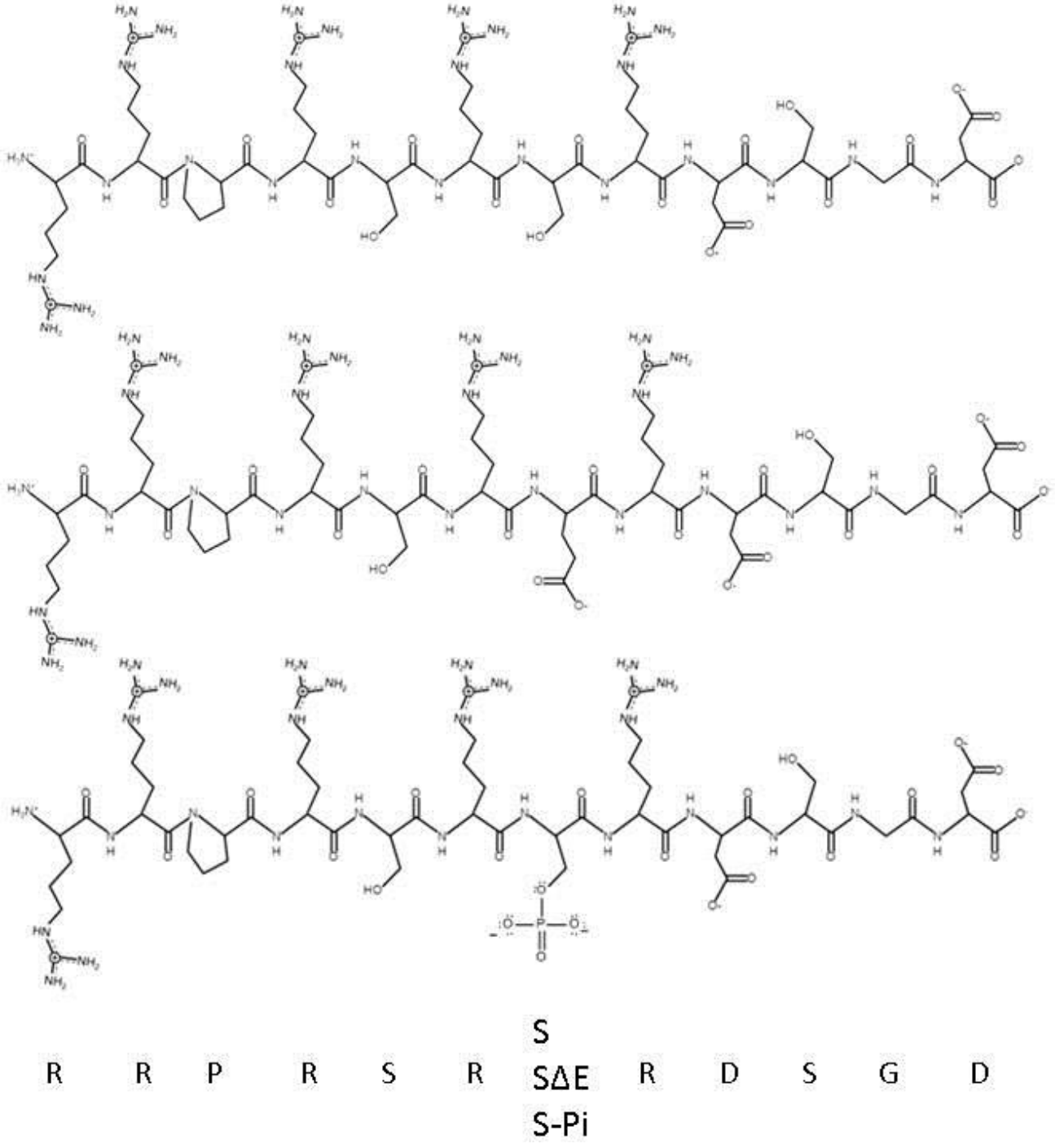

Figure 1.11 Ig34 Linker Region of Wild Type Compared to S507E Mutation

1.4 Overview of the Study

Although the effects of phosphorylation of palladin have been studied briefly *in vivo*, our goal was to determine the specific effects of phosphorylation of palladin *in vitro*. While *in vivo* studies can provide information about the cellular role of palladin, protein-protein interactions cannot be accurately quantified. The advantage of our *in vitro* studies lies in our ability to accurately quantify the effect palladin has on actin bundling and what effect the phosphorylation of the linker region between Ig3 and Ig4 has on its bundling and binding efficiencies. At the same time, we are able to study the effects palladin has on actin polymerization outside of the cellular environment. With such a vast amount of processes going on within a cell, it is often to our advantage to look at a small number of variables in a very controlled environment. Also, considering the different localizations of palladin to different tissue types, we can make broader statements about the post-translational modifications and its effects on the capabilities of the proteins within any type of cell line. Furthermore, by expressing distinct palladin domains responsible for actin binding, we can more accurately determine what part of palladin is being affected by phosphorylation.

At the start of this project we put forth the hypotheses, based on the previous study that showed phosphorylation of palladin increases bundling in cells, that likewise phosphorylation in the Ig34 domain would enhance its direct binding to F-actin [74] and that the phosphorylation of Ig34 would also significantly enhance bundling of F-actin. Also, on the basis of preliminary studies that show palladin causes G-actin to polymerize, we hypothesized that co-incubation would also enhance bundling. Undertaking binding studies of purified palladin and F-actin allows for a more accurate picture as to what effect phosphorylation has on this interaction. This is pertinent bearing in mind the multiple binding partners of palladin and role as a scaffolding

protein. A higher affinity interaction between actin and palladin could be altered by phosphorylation and subsequently have an effect on the role binding partners play in the cell. Through the bundling studies, we are able to not only quantify the effect of phosphorylation but also examine it in a controlled environment outside of the cell lysate, whether these other actin binding proteins may indirectly influence the results. This allows us to determine if it is phosphorylation alone that causes a difference in bundling and consequently causes a change in podosome formation. Finally, the co-polymerization studies allow us to determine the effects, if any, palladin has on filament and bundle formation. This provides us with a better picture of the role of palladin in podosome formation, which likely relies on both polymerization and bundling of actin. By using cosedimentation assays and pure constructs of palladin in both wild type and phosphomimetic forms, a more accurate picture can be drawn of palladin's interaction with actin and how this is affected by Akt1 phosphorylation. These findings are presented in the following chapters in conjunction with the implications they have toward the cellular role of palladin and actin in cancer metastasis.

2. EXPERIMENTAL METHODS

2.1 Isolation of Palladin Domains

All domains of palladin were grown in a Lab Companion IS-971 incubator. Beckman Coulter Allegra 6R and J2-MC centrifuges were used for cell pelleting and supernatant extraction. An AKTA Purifier 900 series FPLC was used for any steps involving FPLC purification. Either custom packed gravity flow nickel affinity columns or a GE HisTrap™ Ni Sepharose High Performance column was used for initial purification from the supernatant cell lysis. Custom-packed Sephacrose S-200 columns were used for S-column affinity purification and a GE HiPrep™ 16/60 Sephacryl S-200 column was used for gel filtration. An Optizen UV/VIS Spectrophotometer was used for monitoring cell growth and measuring DNA or protein concentration. Reagents were purchased through Fisher unless otherwise noted.

2.1.1 Vectors

Protein domains Ig3, Ig3L, and Ig34 were used as defined previously [38]. These domains were cloned into pTBSG, or pTMalE vectors as described previously by Phillip Gao at the University of Kansas, which contain a tobacco etch virus protease recognition site (ENLYFQG) between the desired domain and affinity tags, either a 6His or MBP-6His, respectively [85]. Primers were designed to insert wildtype palladin Ig3L and Ig34 into pTBSG and pTBMalE vectors: 5'-TACTTCCAATCCAATGCGAACGCAACAGCTCCCTTCTTTGAG-3' (forward) and 5'-TTATCCACTTCCAATGTTAAATGGGCTCGTTTTCATCTCCACTG-3' (reverse) for Ig3L. Primers for Ig34 were designed to insert it into pTMalE: 5'-TACTTCCAATCCAATGCGAACGCAACAGCTCCCTTCTTTGAG-3' (forward) and 5'-TTATCCACTTCCAATGTTACTTGTGTGCTTCCTTAGCAGC-3' (reverse). A Fermentas

PCR kit was used (1x GC buffer, 0.2 mM dNTP, 0.5 µM forward primer, 0.5 µM reverse primer, 10ng template DNA (phrGFP-palladin), 3% DMSO, 1 U Phusion Hot Start II High-Fidelity DNA Polymerase) with PCR cycling parameters of: initial denaturation, 98 ºC for 3 min; denaturation, 98 ºC for 30s, annealing, 50 ºC for 30 sec, elongation, 72 ºC 30 sec (30 cycles); final elongation 72 ºC for 5 min; final hold 4 ºC.

The serine to glutamic acid mutation in the linker region at serine 507 was created with the forward primer GGCCTCGCTCTCGAGAACGGGACAGTGGAGATGAAAACG and the reverse primer CGTTTTCATCTCCACTGTCCCGTTCTCGAGAGCGAGGCC (Integrated DNA Technologies). Mutagenic PCR was done with a Fermentas kit (1x GC buffer, 0.2 mM dNTP, 0.5 µM forward primer, 0.5 µM reverse primer, 10 ng template DNA (pTBSG-palladin Ig3L and pTBMalE-palladin Ig34), 3% DMSO, 1U Phusion Hot Start II High-Fidelity DNA Polymerase). Mutagenic PCR parameters were: initial denaturation, 98 ºC for 3 min; denaturation, 98 ºC for 30s, annealing, 55 ºC for 30 sec, elongation, 72 ºC 3.5 min (20 cycles); final elongation 72 ºC for 5 min; final hold 4 ºC.

2.1.2 Growth Methods

Vectors were transformed into either BL21(DE3) CodonPlus-RIPL (Stratagene) or T7 Express LysY cells (New England Biolabs) *Escherichia coli* and transferred to selection plates containing both ampicillin at 50 mg/ml (Gold Biotechnology) and chloramphenicol at 34 mg/ml. 100 mL overnight starter cultures containing LB (5 g yeast extract, 10 g NaCl, 10 g tryptone, 1 L water), 50 mg/ml ampicillin, and 34 mg/ml chloramphenicol were prepared and started with a single colony from selection plates and grown overnight at 37 ºC. 10 mL of these overnights was transferred to 2.8 L flasks containing 1 L LB, 50 mg/ml ampicillin, and 34 mg/ml chloramphenicol, and grown at 37 ºC in a Lab Companion IS-971 incubator until the OD_{600} =

~0.7. At this point the temperature was dropped to 18 ºC and 0.5 mM IPTG (Gold Biotechnology) was added to the culture to induce protein expression and allowed to grow overnight. These cells were spun down in a Beckman Coulter Allegra 6R centrifuge the next day and resuspended in Lysis Buffer (25 mM Tris pH 7.5, 100 mM NaCl, 5 mM imidazole (Acros Organics) [and 5% glycerol, 5 mM L-arginine for domains over 20 kDa]), 50 mL per 4 L of growth. At this point BAL and PMSF (Acros Organics) protease inhibitors were added (1 mM phenylmethylsulfonyl fluoride, and 1X BAL (1000X BAL = 10 mg/ml benzamidine, 2 mg/ml antipain (CalBiochem), and 1 mg/ml leupeptin)).

2.1.3 Purification Methods

Cells were lysed for 1 hour by sonication (5s on, 5s off) on a Fisher Scientific FB120 sonicator at 100% amplitude and then spun at 18,000 rpm (25k x g) in a Beckman Coulter J2-MC centrifuge equipped with a JA-20 rotor for 45 minutes. The supernatant for domains under 20 kDa was then run over gravity flow nickel affinity columns (packed with Thermo His-Pur™ Ni-NTA Resin) and washed with 100 mL of Wash Buffer (25 mM Tris pH 7.5, 100 mM NaCl, 25 mM imidazole) and eluted with 50 mL of Elution Buffer (25 mM Tris pH 7.5, 100 mM NaCl, 500 mM imidazole). For domains over 20 kDa, a GE HisTrap™ Ni Sepharose High Performance column was used and a 10 column volume gradient ran from 5 to 100% Lysis Buffer B (25 mM Tris pH 7.5, 100 mM NaCl, 500mM imidazole, 5% glycerol, 5 mM L-arginine). TEV protease was added directly to the eluted protein domains which were under 20 kDa and allowed to cut overnight at 4 ºC whereas domains over 20 kDa were allowed to cut overnight at room temperature with the addition of 0.4 M NaCl, 1 mM PMSF, 1X BAL, 2 mM EDTA, and 20 mM DTT (Bioworld). Removal of the affinity tag was confirmed by SDS-PAGE and the eluted fraction was then diluted to 100 mL with S-Column Buffer A (25 mM KH_2PO_4 pH 5.5, 100 mM

NaCl, 2 mM DTT, [and 5% glycerol, 5 mM L-arginine, 2 mM EDTA for domains over 20 kDa]). This was run over an S-Column and eluted by a 0 to 100% gradient of S-column B buffer (25 mM KH_2PO_4 pH 5.5, 1 M NaCl, 2 mM DTT, [and 5% glycerol, 5 mM L-arginine, 2 mM EDTA for domains over 20 kDa]). Proteins under 20 kDa were then dialyzed into the necessary buffer for use in assays, whereas the domains over 20 kDa were dialyzed into buffer containing 0.1 M NaCl, 25 mM HEPES pH 7.5, 4 mM DTT, 2 mM EDTA, and 5% glycerol.

The larger domains, over 20 kDa, were then concentrated to less than 5 mL total volume and the NaCl concentration was increased to 0.75 M. This concentrated sample was then run over a GE HiPrep^{TM} 16/60 Sephacryl S-200 gel filtration column in buffer containing 0.75 M NaCl, 25 mM HEPES pH 7.5, 4 mM DTT, 2 mM EDTA, and 5% glycerol. The most pure fractions, as assessed by SDS-PAGE, from gel filtration were collected and then dialyzed into the necessary buffer for usage in assays. Protein concentration was determined using an Optizen UV/VIS spectrophotometer to measure absorbance at 280 nm. The extinction coefficients for Ig3 and Ig3L are 11,585 $M^{-1}cm^{-1}$, 7,115 $M^{-1}cm^{-1}$ for Ig4, and 18, 825 $M^{-1}cm^{-1}$ for Ig34.

2.2 Actin Isolation

Monomeric actin was purified by methods adapted from Spudich and Watt [86]. Rabbit muscle acetone powder (PelFreeze) was mixed with 20 ml pre-chilled G-buffer (0.2 mM ATP, 0.2 mM $CaCl_2$, 2 mM Tris/HCl, pH 8.0, 0.5 mM DTT for each gram of muscle acetone powder and stirred for 30 minutes at 4 °C. This suspension was centrifuged in a Beckman Coulter J2-MC with a JA-20 rotor at 16,000 rpm for 30 minutes at 4 °C. The supernatant was filtered through glass wool and 50 mM in KCl and 2 mM $MgCl_2$ and 1 mM ATP were added on ice. This allowed actin to polymerize, at room temperature for 30 minutes and then at 4°C for 90 minutes while stirring. The concentration of KCl was increased at this time to 0.8 M. This solution was

then centrifuged for 2 hours in Ti-45 rotor at 35,000 rpm at 4 °C in a Beckman Coulter Optima LE-80K Ultracentrifuge. The pellets were rinsed once with G-buffer and transferred to a dounce homogenizer with loose pestle. The pellet was suspended in 3 ml of G-buffer per gram of acetone powder, homogenized, then dialyzed into G-buffer with DTT for 2 to 3 days to depolymerize. This was centrifuged in a Ti-70.1 rotor for 2 hours at 37,000 rpm in the LE-80K Ultracentrifuge. The supernatant was then gel filtered over a GE HiPrep^{TM} 16/60 Sephacryl S-200 column with G-buffer. The back portion of the chromatogram peak was used for co-sedimentation assays and snap frozen in liquid nitrogen. Concentration was determined using an Optizen UV/VIS spectrophotometer to measure absorbance at 290 nm with the extinction coefficient 26,600 $M^{-1}cm^{-1}$.

2.3 Co-Sedimentation Assay (F-actin or G-actin conditions)

Co-Sedimentation assays were all carried out at room temperature in a Beckman Coulter Airfuge CLS Ultracentrifuge. 100µL total volume was prepared for both binding and bundling assays in either ultracentrifuge tubes or 1.5mL microcentrifuge tubes in the case of bundling assays. The general scheme is depicted in Figure 2.1. Buffers used were either polymerization buffer, or F-Buffer (2X, 20 mM Tris pH 7.5, 200 mM KCl, 4 mM $MgCl_2$, 4 mM DTT) or G-Buffer (0.2 mM ATP, 0.2 mM $CaCl_2$, 2 mM Tris/HCl pH 7.5). The statistical difference of percent actin in the bundles was compared by two tailed, paired t-test (e.g. 10 µM Actin & 10 µM Ig3). The values are a probability of the null hypothesis being void. Therefore a low value, below 0.05 (the 5% significance level) denotes that the null hypothesis is not supported, in this case that the groups are not significantly different.

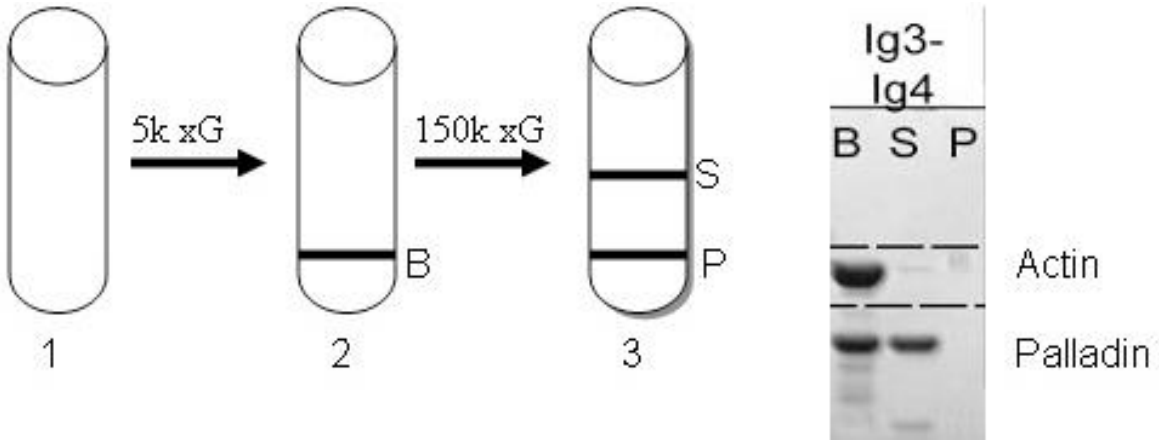

Figure 2.1 Co-sedimentation Assay. During the binding assay the slow speed spin is eliminated and only supernatant and pellet are obtained.

2.3.1 Binding Assay

Monomeric actin stocks stored at -80 °C were diluted by one-half with 2X F-Buffer and allowed to polymerize for 30 minutes. In 100µL total volume was prepared directly in ultracentrifuge tubes with 5 µM actin and necessary concentrations of palladin domain. Palladin was in either 1X polymerization buffer for domains under 20 kDa and in storage buffer (25 mM HEPES pH 7.5, 100 mM NaCl, 5% glycerol, 5 mM DTT) for domains over 20 kDa. Total volume was increased to 100 µL with 1X F-Buffer after addition of proteins and allowed to incubate at room temperature for one hour. This was done in triplicate, at least. These preparations were then spun at 150,000 *x g* in the Airfuge for 30 minutes. The supernatant was then carefully removed and 100 µL of 2X Tris-glycine electrophoresis buffer (1X, 25 mM Tris pH 8.3, 250 mM glycine, 0.1% SDS) was added to the pellet. 35 µL of 4X loading buffer (4X, 200 mM Tris pH 6.8, 8% SDS, 40% glycerol, 4% β-mercaptoethanol, 0.08% bromophenol blue, 400 mM DTT) was added to these 100 µL supernatant and pellet volumes. This was boiled and then ran on 12% SDS-PAGE for 45 minutes at 200 volts. The resulting gels were stained and destained with SafeBlue stain, scanned with a Canon LiDE 110 and the bands of protein were

quantified on ImageJ software [87]. The normalized densitometry of bound palladin in the pellet was found using Equation 1.

$$Y = a + \frac{(D-A)(b-a)}{(B-A)} \quad (1)$$

Where Y is the normalized pellet densitometry of palladin on an arbitrary scale from 0 to 100, where 0 is the minimal normalized binding and 100 is our maximal normalized densitometry. D is the raw densitometry reading. A and B are the raw minimal and maximal densitometry readings, respectively, for a single data set of the three trials. Lower case a and b are the minimal and maximal, respectively, normalized densitometry readings on the 0 to 100 scale. These triplicate values for palladin in the pellet, bound palladin, (Y-axis values) were plotted against the known concentrations of palladin aliquoted into each sample, as determined by UV/VIS. The resulting curve was analyzed using GraphPad Prism version 5.0b for Mac, GraphPad Software, San Diego, California, USA, www.graphpad.com. A non-linear regression (curve fit) was used with one site-total binding, which includes contribution from non-specific binding. The model used is shown in Equation 2. Y is the normalized pellet densitometry of palladin and NS is nonspecific binding. Background was restrained to 0 because the lowest normalized densitometries at 0.5 μM are 0.

$$Y = \frac{Bmax(\mu M\ Palladin\ total)}{Kd + Bmax(\mu M\ Palladin\ total)} + NS(\mu M\ Palladin\ total) + Background \quad (2)$$

2.3.2 Bundling Assay

Actin stocks were diluted in half with 2X F-Buffer and allowed to polymerize for 30 minutes. A 100 μL total volume was prepared in 1.5 mL ultracentrifuge tubes with 10 μM actin and necessary concentrations of palladin domain. Palladin was in either 1X polymerization

buffer for domains under 20 kDa and in storage buffer (25 mM HEPES pH 7.5, 100 mM NaCl, 5% glycerol, 5 mM DTT) for domains over 20 kDa. No difference was observed in using these two buffers. Volume was increased to 100 µL after addition of proteins and allowed to incubate at room temperature for one hour. This was done in triplicate, at least. These preparations were then spun at 5,000 x *g* in a Beckman Coulter Microfuge™ 16 Centrifuge. The supernatant was removed and 100 µL 2X Tris-glycine electrophoresis buffer added to the pellet. The supernatant was added to an ultracentrifuge tube and spun at 150,000 x *g* in the Airfuge for 30 minutes. The supernatant was then carefully removed and 100 µL of 2X Tris-glycine electrophoresis buffer (1X, 25 mM Tris pH 8.3, 250 mM glycine, 0.1% SDS) was added to the pellet. 35 µL of 4X loading buffer (4X, 200 mM Tris pH 6.8, 8% SDS, 40% glycerol, 4% β-mercaptoethanol, .08% bromophenol blue, 400 mM DTT) was added to these 100 µL supernatant and pellet volumes. This was boiled and then ran on 12% SDS-PAGE for 45 minutes at 200V. The resulting gels were stained and destained with SafeBlue stain, scanned with a Canon LiDE 110, and the bands of protein in the bundle, supernatant, and pellet were quantified on ImageJ software [87].

2.3.3 Co-Polymerization Binding and Bundling Assays

Two types of co-polymerization assays were carried out to observe polymerization of G-actin by palladin. Palladin and monomeric actin were incubated and then spun at 150,000 x *g* for direct binding cosedimentation or incubated and then spun at both 5,000 xg and 150,000 x *g* for bundling cosedimentation. For the binding co-polymerization assays, 5 µM of monomeric actin (without the addition of polymerization buffer) was added to ultracentrifuge tubes with necessary concentrations of palladin and 100 µL total volume of G-buffer. Palladin was in either G-buffer for domains under 20 kDa and storage buffer for domains over 20 kDa, neither of which contain the $MgCl_2$ or KCl necessary for initiation of actin polymerization. This mixture was allowed to

co-incubate for one hour and then spun at 150,000 x *g*. The binding protocol was then followed as normal, in triplicate. For the bundling co-incubation, 10 μM actin was added to a 1.5 mL microcentrifuge tubes with necessary concentrations of palladin and 100 μL total volume of G-buffer. Palladin was in either G-buffer for domains under 20 kDa and storage buffer for domains over 20 kDa. This was allowed to co-incubate for one hour and then spun at 5,000 x *g* and then 150,000 x *g*, with the bundling protocol being followed as normal, in triplicate.

2.4 Fluorescence Microscopy

For fluorescence microscopy, a Nikon Eclipse E800 Microscope was used on the FITC-HYQ setting (excitation 460-500 nm, dichroic mirror 505, Barrier filter 510-560) with a Nikon Plan Apo Lense objective (100x/1.40 Oil, DIC H, infinity/0.17, WD 0.13). A Photometrics CoolSNAP EZ, Turbo 1394 camera was used for image acquisition and an X-Cite Series 120 PC laser used for illumination. MetaMorph imaging software series 7.6.30 was used for image acquisition. Cytoskeleton Acti-stain 488 phalloidin was used at 66.6 μM resuspended in 100% methanol. Imaging buffers were prepared as follows: (1X polymerization imaging buffer; 10 mM Tris, 100 mM KCl, 2 mM $MgCl_2$, 2.5 mM DTT, pH 7.5, 1% methylcellulose, 30 mM Glucose (Sigma), 100 μM DTT, 0.4 μM ATP, 0.040 mg/mL Catalase, and 0.2 mg/mL Glucose Oxidase) (G-imaging buffer; 2.0 mM Tris, 0.2 mM ATP, 0.2 mM CaCl2, 0.5mM DTT, 25mM NaCl, pH 7.5, 1% methylcellulose, 30 mM Glucose, 100 μM DTT, 0.4 μM ATP, 0.040 mg/mL Catalase, and 0.2 mg/mL Glucose Oxidase).

2.4.1 G-Buffer Fluorescence Microscopy

10 μM Actin was incubated 60 minutes with the necessary concentration of palladin in 100 μL total volume of G-buffer (2.0 mM Tris, 0.2 mM ATP, 0.2 mM $CaCl_2$, 0.5mM DTT, 25mM NaCl, pH 7.5) This was then diluted 10 times in G-imaging buffer and phalloidin was

added to 2 μM and allowed to incubate two minutes. 5 μL of sample was then dropped on a microscope slide, covered with a cover slip, and then imaged immediately.

2.4.2 F-Buffer Fluorescence Microscopy

Actin was polymerized for 30 minutes in 1X polymerization buffer (10 mM Tris, 100 mM KCl, 2 mM $MgCl_2$, 2 mM DTT, pH 7.5). The necessary concentration of palladin, 10 μM actin, and 1X polymerization buffer was mixed in a 1.5 mL microcentrifuge tubes and allowed to incubate for 1 hour at room temperature. This was then diluted 10 times in 1X polymerization imaging buffer and phalloidin was added to 2 μM and allowed to incubate two minutes. 5 μL of sample was then dropped on a microscope slide, covered with a cover slip, and then imaged immediately.

2.5 Electron Microscopy

Electron microscopy was carried out at the University of Virginia in the Egelman lab by Albina Orlova. G-actin from rabbit muscle was used after thawing and dialyzing into G-buffer solution (5 mM Hepes, pH 7.5, 0.2 mM $CaCl_2$, 1% NaN_3, 1 mM ATP, 2 mM DTT) just before the experiment was carried out. The protein was clarified by centrifugation in a TLX-tabletop centrifuge at 120,00 rpm for 1 hour and 2/3 top of supernatant was used during 2-3 days, storing actin in ice. For copolymerization experiments 2-3 μM of G-actin was mixed with 20-30 μM of palladin fragment Ig34. After 7-15 minutes of incubation, the solution was applied on carbon-covered discharged copper grids and stained by 2% of uranyl acetate. Images were collected on CCD-digital camera using Tecnai-12 electron microscope (FEI) at 80 kV and 30,000X magnification.

2.6 Analytical Ultracentrifugation

Analytical ultracentrifugation was carried out as previously described by Yasuaki Hiromasa at Kansas State University [88]. Sedimentation velocity experiments were conducted using an Optima XL-1 ultracentrifuge using an An-60 Ti rotor at 4 °C in storage buffer (25 mM HEPES pH =7.5, 100 mM NaCl, 5% glycerol, 5 mM DTT). Sedimentation was monitored at 280 nm using double sector cells with a final loading of 400 µl per cell. Sedimentation was at 50,000 rpm with scans made at 6 minute intervals over one hour. Sedimentation data were analyzed using DCDT+ software version 1.16 and sedimentation coefficients calculated using *g(s*)* fitting function in DCDT+ software. Buffer density and viscosity were calculated by Sednterp version 1.08 and the partial specific volumes of proteins were calculated from their amino acid composition using Sednterp as well. Software is available from the RASMB website (www.rasmb.org) [88, 89].

3. RESULTS

3.1 Binding Studies of Palladin Domains

To compare the actin-binding affinity of the various Ig domains of palladin to determine the effects of the phosphomimetic mutation, the concentration of polymerized actin was held constant at 5 μM and increasing amounts of palladin were used in the binding co-sedimentation assay. We carried out these assays for Ig3 (Figure 3.1), Ig3L and Ig3L P (Figure 3.2), as well as Ig34 and Ig34 P (Figure 3.3), all under the polymerizing conditions of F-buffer. The bands of palladin in the pellet were quantified, giving us a raw densitometry reading. These raw values of bound palladin in the pellet were normalized as described in the experimental methods section. The known total concentration (X-axis) was plotted against the normalized pellet densitometry of bound palladin (Y-axis).

Gels for these assays showed most of the actin in filamentous form and sedimenting to the pellet as expected. Representative gels for these assays are shown in Figures 3.1 through 3.3. The average binding curve and associated fit to single site total binding model, that allows for both specific binding at a single site and nonspecific binding, are shown as well, obtained as described in the experimental section. Equilibrium dissociation constants, K_d, values are also presented in Table 3.1. Ig34 and Ig34 P K_d values obtained in this study describe a tighter binding affinity than those of ~9 μM previously found by Dixon, *et al.*, but what we can surmise from this data as a whole is Ig34 and Ig34 P have a higher affinity for F-actin than Ig3 or Ig3L [38].

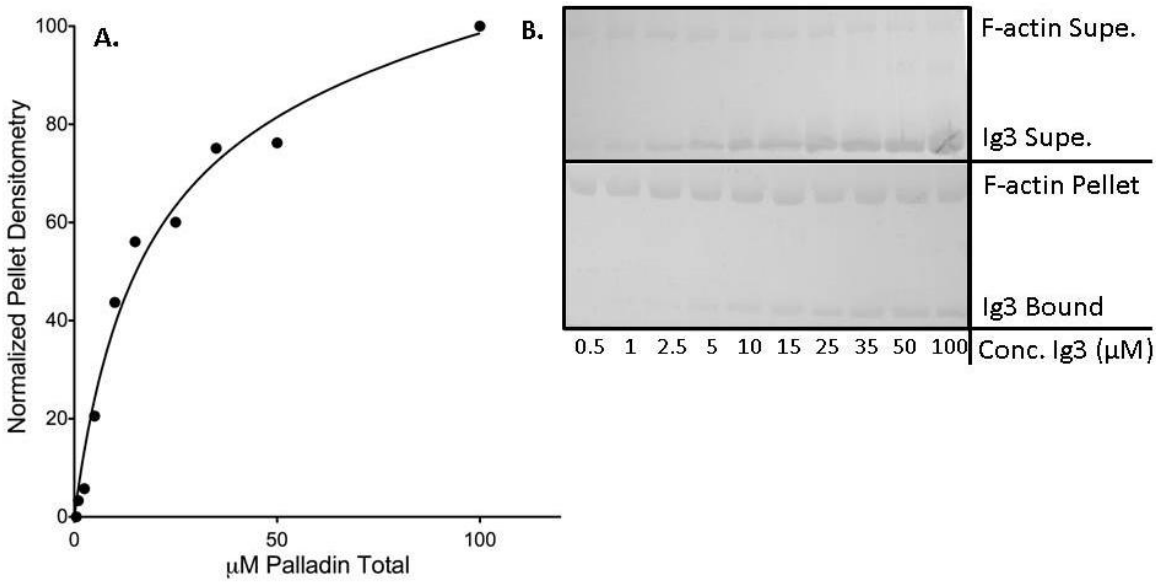

Figure 3.1. Ig3 Binding to Actin. 5µM actin was incubated with increasing amounts of the Ig3 domain of palladin (filled circles). A) The resulting K_d is 16.3 ± 6.8 µM. B) Representative SDS-PAGE of binding assay for Ig3.

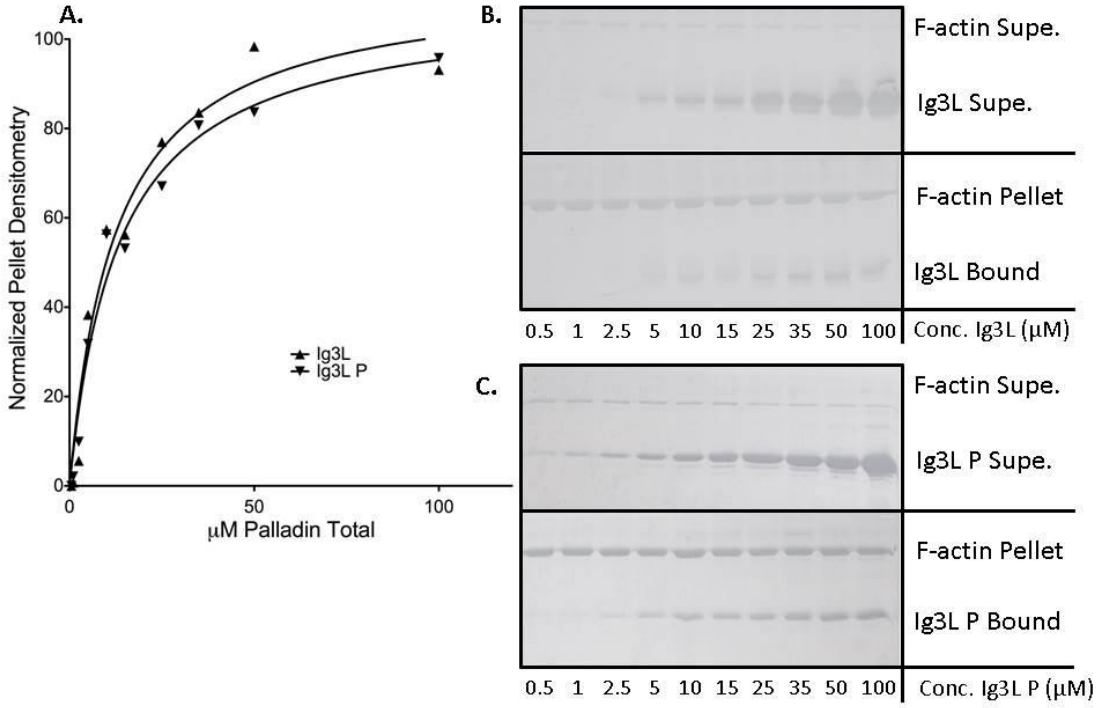

Figure 3.2. Ig3L Binding to Actin. 5µM actin was incubated with increasing amounts of the Ig3L (triangles) and Ig3L P (upside down triangles) domain of palladin. A) The resulting K_d values are 12.4 ± 3.6 µM and 13.2 ± 4.2 µM. B) Representative SDS-PAGE of binding assay for Ig3L. C) Representative SDS-PAGE of binding assay for Ig3L P.

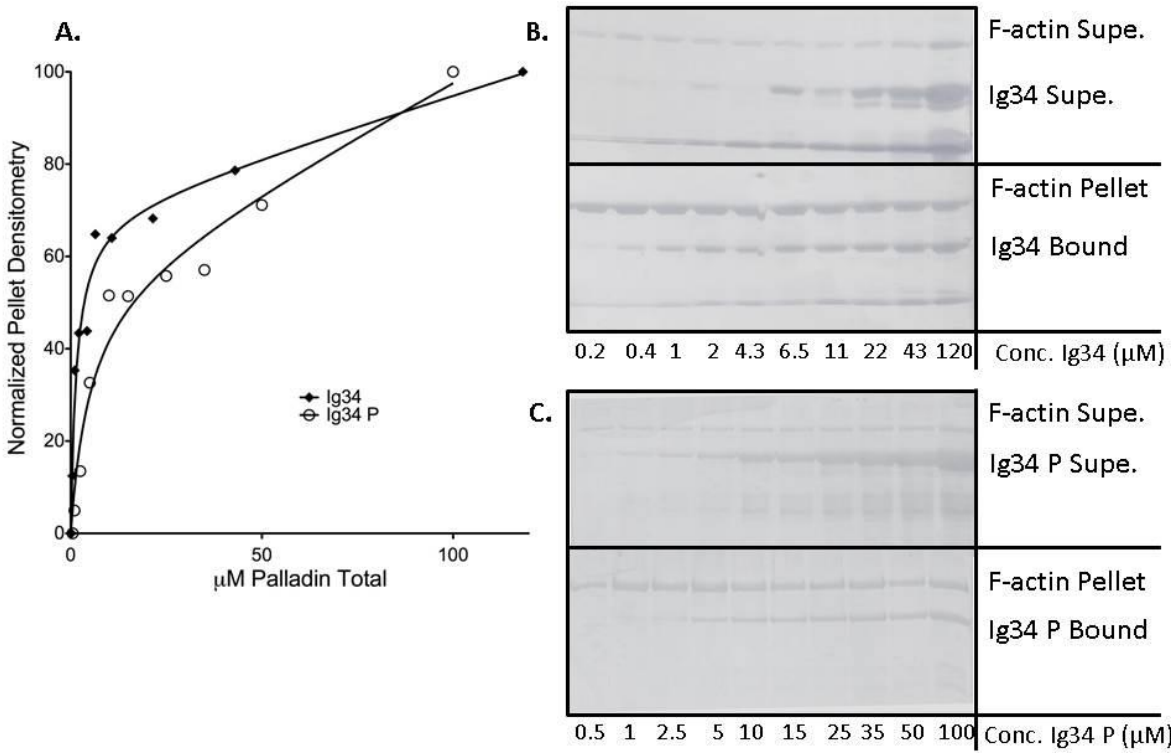

Figure 3.3. Ig34 Binding to Actin. 5μM actin was incubated with increasing amounts of the Ig34 (diamonds) and Ig34 P (circles) domain of palladin. A) The resulting K_d values are 1.5 ± 0.4 μM and 5.1 ± 1.9 μM. B) Representative SDS-PAGE of binding assay for Ig34. C) Representative SDS-PAGE of binding assay for Ig34 P.

TABLE 3.1

F-BUFFER BINDING PARAMETERS FOR VARIOUS PALLADIN CONSTRUCTS

Construct	K_d (μM)	pI
Ig3	16.3 ± 6.8	9.30
Ig3*	70 ± 10	9.30
Ig3L	12.4 ± 3.6	9.62
Ig3L P	13.2 ± 4.2	9.47
Ig34	1.5 ± 0.4	9.28
Ig34*	8.7 ± 1.5	9.28
Ig34 P	5.1 ± 1.9	9.17
90 kDa	2.1 ± 0.5	N/A

* -denotes previously determined value by Dixon et al. [38]

3.2 Bundling Studies of Palladin Domains

To determine the bundling efficiency of the various domains, the concentration of polymerized actin was held constant at 10 μM and increasing amounts of palladin were used in

the bundling co-sedimentation assay. The bands of F-actin in the SDS-PAGE were quantified and then the percent of F-actin in the bundle, supernatant, and pellet were calculated as fractions of the total F-actin band intensity. This allows us to eliminate deviations in the extent of SDS-PAGE staining and destaining.

We carried out these assays for Ig3, Ig4, and Ig3 with Ig4 to determine the bundling efficiency of Ig3 and if the separate Ig4 domain could increase bundling when incubated with Ig3, as shown in Figure 3.4. Ig4 displayed the same amount of bundled F-actin as F-actin alone. Ig3 with Ig4 displayed the same amount of bundled F-actin as the same concentration of Ig3 alone. Ig3 displayed increasing bundling from 5 to 20 μM concentrations and significantly greater bundling at 10 and 20 μM as surmised from T-test values shown in Table 3.2, numbers 1 through 5.

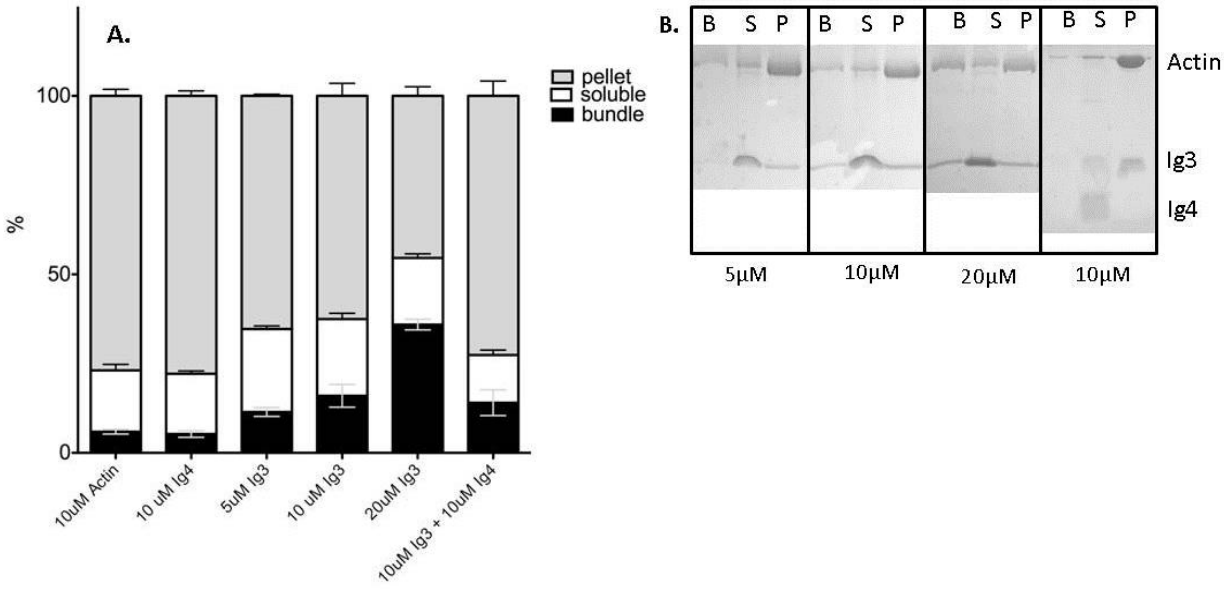

Figure 3.4. Ig3 Bundling of Actin. A) 10 μM actin was incubated with increasing amounts of the Ig3 domain of palladin. Ig4 was also used alone and in conjunction with Ig3 to determine if its presence increases bundling. B) Representative SDS-PAGE of bundling assay for Ig3.

We then carried out these assays for Ig3L, Ig3L P, and Ig3L with Ig4 to determine if the phosphomimetic increased bundling and if the addition of the separate Ig4 domain could increase

bundling when incubated with Ig3L, as shown in Figure 3.5. Ig3L displayed the same amount of bundled F-actin when incubated with Ig4. Ig3L P and Ig3L also displayed similar bundling efficiencies and were not significantly different given the T-test values in Table 3.2, numbers 6 through 9.

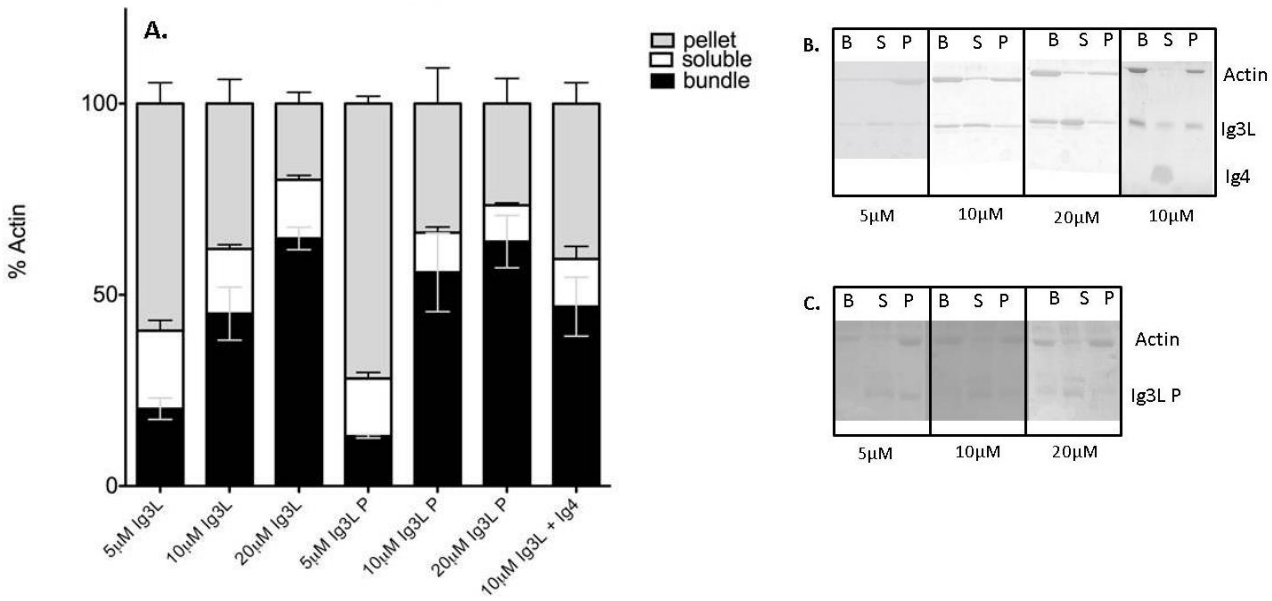

Figure 3.5. Ig3L Bundling of Actin. A) 10μM actin was incubated with increasing amounts of the Ig3L and Ig3L P domain of palladin. Ig4 was also used in conjunction with Ig3L to determine if its presence increases bundling. B) Representative SDS-PAGE of bundling assay for Ig3L. C) Representative SDS-PAGE of bundling assay for Ig3L P.

We then carried out these assays for Ig34 and Ig34 P to determine if the phosphomimetic increased bundling, as shown in Figure 3.6. Ig34 P displayed an increased amount of bundled F-actin compared to the wild type Ig34 at lower concentrations, indicated by a pairwise analysis, but these were not statistically different as indicated by a low T-test value in number 10 in Table 3.2. Since we had impurities within both samples of wild type Ig34 and Ig34 P, similar to previous studies, we added the gel filtration step to our purification scheme and carried out a differential bundling assay with Ig34 and Ig34 P [38].

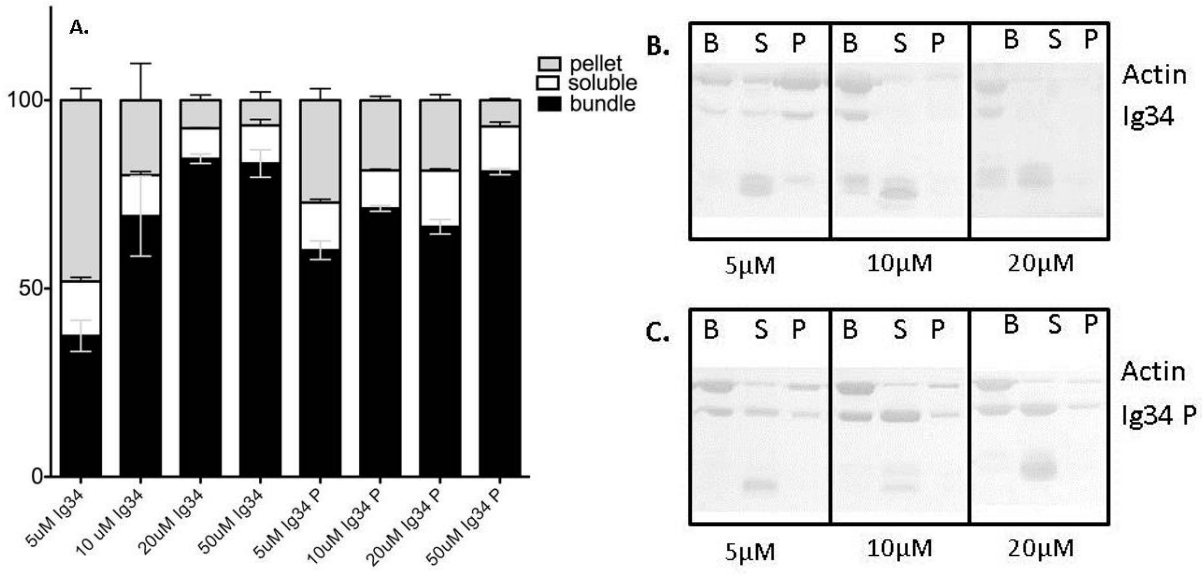

Figure 3.6. Ig34 Bundling of Actin. A) 10 μM actin was incubated with increasing amounts of the Ig34 and Ig34 P domain of palladin. These are the results of initial studies done. B) Representative SDS-PAGE of bundling assay for Ig34. C) Representative SDS-PAGE of bundling assay for Ig34 P.

In utilizing the differential bundling assay, a greater range of concentrations of palladin were accounted for and a more accurate picture of bundling efficiency of F-actin could be obtained. Ig34 P bundles F-actin with greater efficiency at all concentrations until a 1:2 molar ratio of palladin to F-actin is reached, as shown in Figure 3.7. These are significantly different until this 1:2 molar ratio, as indicated in Table 3.2 number 18, and then both wild type Ig34 and Ig34 P bundle F-actin with similar efficiencies, indicating a saturating bundling concentration has been reached. Percent actin bundled begins around 10% to 15% as this is the background level normally attained.

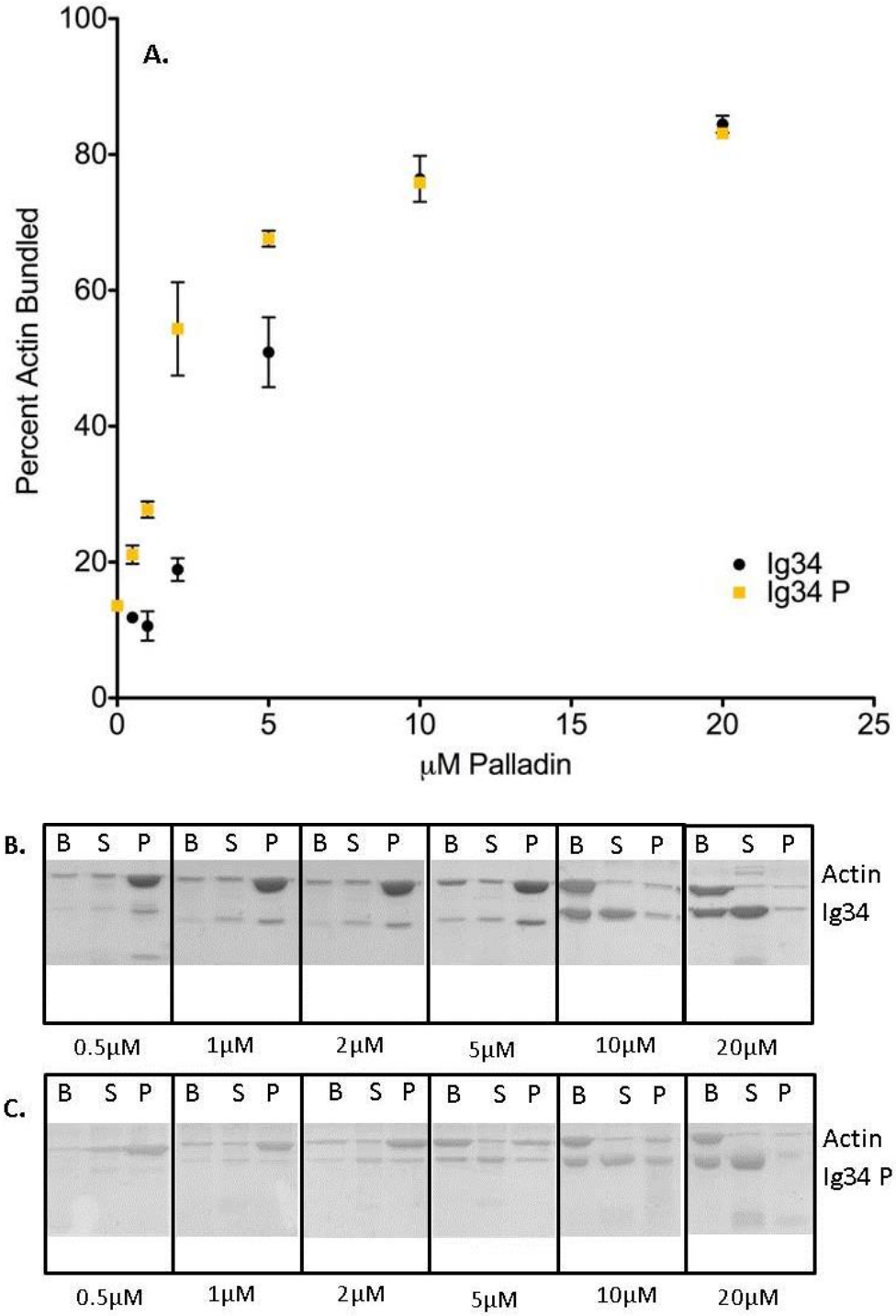

Figure 3.7. Ig34 Differential Bundling of Actin. A) 10 μM actin was incubated with increasing amounts of the Ig34 (black circles) and Ig34 P (yellow squares) domain of palladin. These results show the bundling difference at a wider range of concentrations. B) Representative SDS-PAGE of bundling assay for Ig34. C) Representative SDS-PAGE of bundling assay for Ig34 P.

TABLE 3.2

T-TEST VALUES FOR F-BUFFER BUNDLING ASSAYS

Ref. #	Comparison	T-Test
1	10 μM Actin & 10 μM Ig4	0.580
2	10 μM Actin & 5 μM Ig3	0.088
3	10 μM Actin & 10 μM Ig3	0.013
4	10 μM Actin & 20 μM Ig3	0.005
5	10 μM Ig3 & (10 μM Ig3 + 10 μM Ig4)	0.278
6	5 μM Ig3L & 5 μM Ig3L P	0.139
7	10 μM Ig3L & 10 μM Ig3L P	0.059
8	20 μM Ig3L & 20 μM Ig3L P	0.212
9	10 μM Ig3L & (10 μM Ig3L + 10 μM Ig4)	0.854
10	5 μM Ig34 & 5 μM Ig34 P	0.065
11	10 μM Ig34 & 10 μM Ig34 P	0.863
12	20 μM Ig34 & 20 μM Ig34 P	0.012
13	50 μM Ig34 & 50 μM Ig34 P	0.533
	Differential Assay, Ig34 & Ig34 P	
14	0 μM	x
15	0.5 μM	0.033
16	1 μM	0.028
17	2 μM	0.023
18	5 μM	0.112
19	10 μM	0.877
20	20 μM	0.289

3.3 Polymerization of Actin by Palladin

To study the effects palladin has on actin in its monomeric state, we carried out co-polymerization assays, where palladin constructs were incubated with G-actin under non-polymerizing conditions. Filaments were not created with a polymerization step before the addition of palladin domains as in the previous binding and bundling assays. Co-sedimentation assays were used to quantify polymerization and bundling efficiency with both wild type and phosphomimetic Ig domains. Fluorescence microscopy was also used to visualize these F-actin filaments and bundles in solution. Finally, electron microscopy was carried out with Ig34 in an

attempt to visualize F-actin bundle formation to determine whether these were parallel bundles or cross-linked bundles as distinguished in Figure 1.3.

3.3.1 Co-Polymerization Assays

Initial co-polymerization cosedimentation assays were carried out with 5 μM G-actin and increasing amounts of Ig3 and Ig3L. The G-actin in this case was mixed with palladin, under G-buffer conditions. Filaments were not pre-formed by polymerization in F-buffer. The bands of actin in the supernatant and pellet were quantified and molar fraction of actin in the pellet was calculated. The polymerization curves for various constructs are shown in Figure 3.8. Nearly all G-actin was polymerized upon the addition of 5 μM of palladin as shown in Figure 3.8.A. Figure 3.8.B shows that Ig3L sediments at a 2:1 palladin to actin ratio when co-polymerized while Ig3 and Ig34 sediment in 1:1 ratios when the concentration reaches 10 μM.

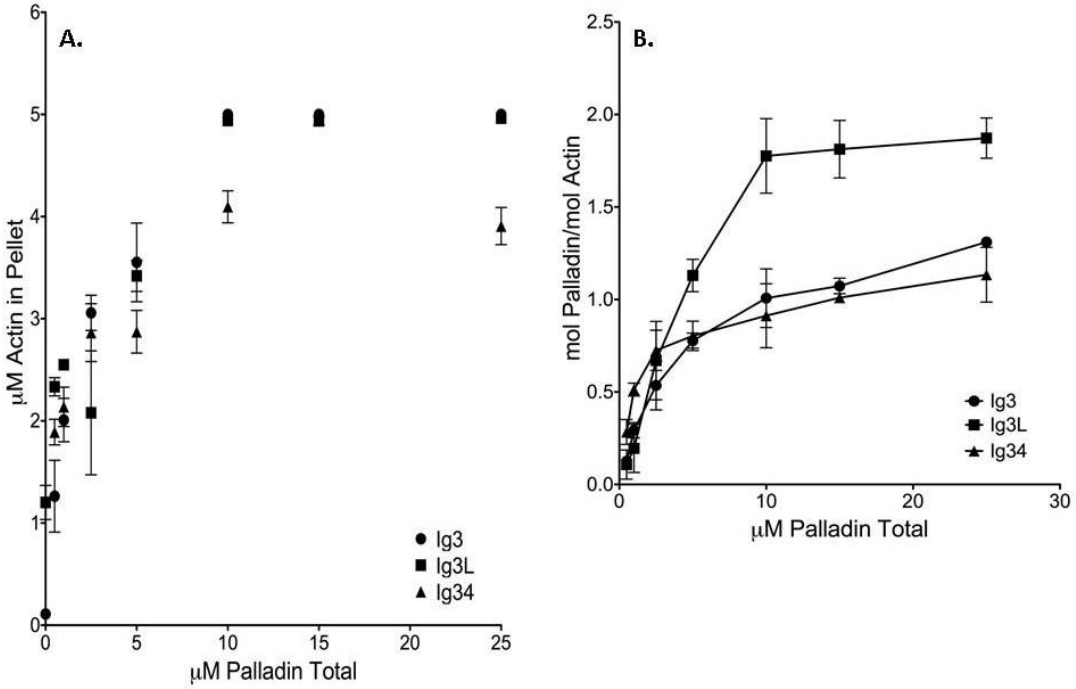

Figure 3.8. Ig3, Ig3L, and Ig34 Co-Polymerization Binding Assay. A) Extent of polymerization when 5 μM G-actin was incubated with increasing amounts of the Ig3 (black circles) and Ig3L (black squares) and Ig34 (black triangles) domain of palladin. B) The molar ratio with 5 μM actin. Data points without error bars indicate that all actin at that point had been polymerized and there was no difference between replicates.

Co-polymerization bundling assays were then carried out with 10 μM G-actin and increasing amounts of Ig3 under non-polymerizing buffer conditions. This is compared with bundling assays done under polymerizing conditions. The results, in Figure 3.9, show that Ig3 is capable of polymerizing and bundling actin with greater efficiency when it is allowed to co-polymerize with G-actin. The T-test values are summarized in Table 3.3.

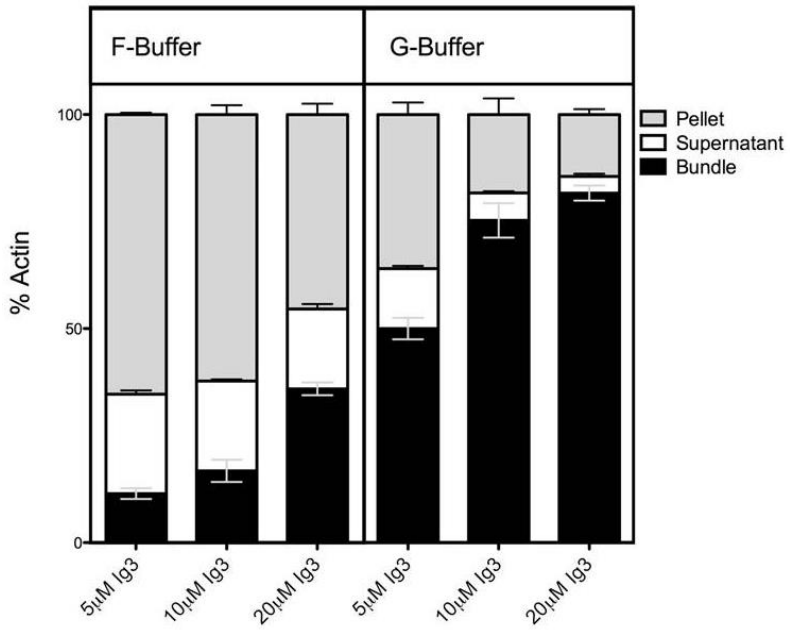

Figure 3.9. Ig3 Co-Polymerization Bundling Assay. 10 μM G-actin was incubated with increasing amounts of the Ig3 domain of palladin in both F-Buffer and G-Buffer. Bundling efficiency is markedly increased when actin is incubated in G-buffer in the presence of palladin.

When Ig3L and Ig3L P are allowed to co-polymerize with 10 μM G-actin, they are both able to bundle actin with greater efficiency than when incubated with polymerized actin and are not significantly different, as summarized in Table 3.4 and depicted in Figures 3.10 and 3.11.

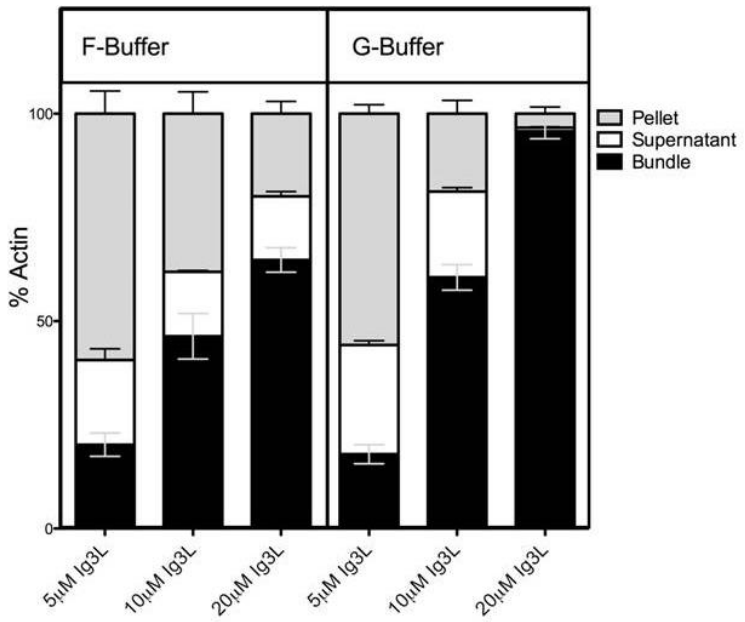

Figure 3.10. Ig3L Co-Polymerization Bundling Assay. 10 μM G-actin was incubated with increasing amounts of the Ig3L domain of palladin in both F-Buffer and G-Buffer. Bundling efficiency is slightly increased when actin is incubated in G-buffer in the presence of palladin.

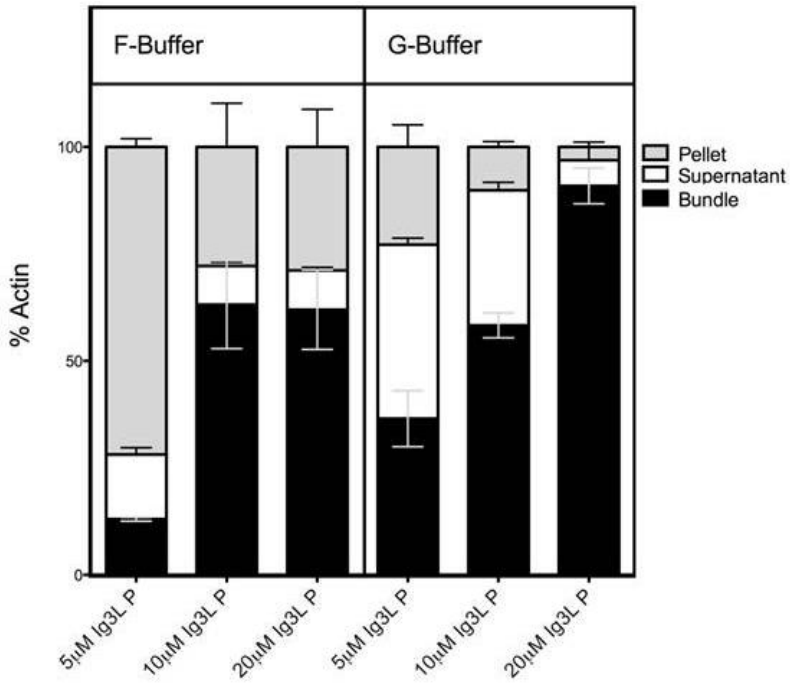

Figure 3.11. Ig3L P Co-Polymerization Bundling Assay. 10 μM G-actin was incubated with increasing amounts of the Ig3L P domain of palladin in both F-Buffer and G-Buffer. Bundling efficiency is slightly increased when actin is incubated in G-buffer in the presence of palladin.

When Ig34 and Ig34 P are allowed to co-polymerize with 10 μM G-actin, they are both able to bundle actin with slightly better efficiency than when incubated with polymerized actin as depicted in Figures 3.12 and 3.13. The bundling efficiency is already substantially higher though than Ig3, Ig3L, or Ig3L P under any conditions.

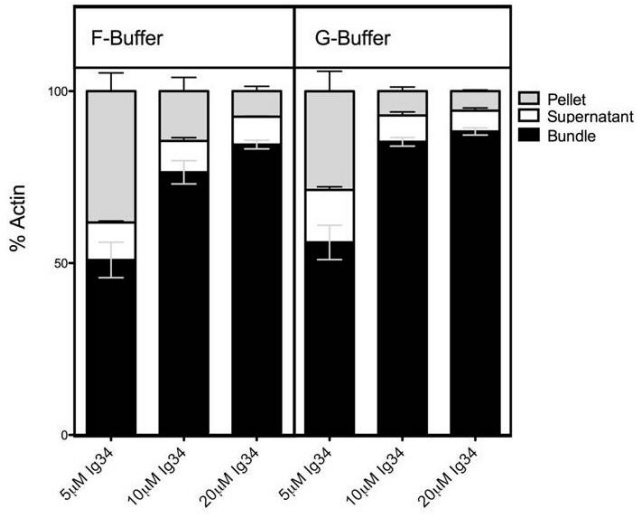

Figure 3.12. Ig34 Co-Polymerization Bundling Assay. 10 μM G-actin was incubated with increasing amounts of the Ig34 domain of palladin in both F-Buffer and G-Buffer. Bundling efficiency is slightly increased when actin is incubated in G-buffer in the presence of palladin.

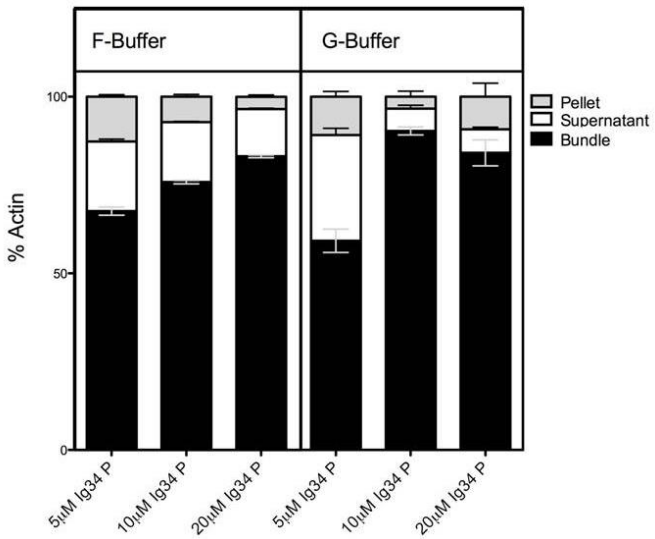

Figure 3.13. Ig34 P Co-Polymerization Bundling Assay. 10 μM G-actin was incubated with increasing amounts of the Ig34 P domain of palladin in both F-Buffer and G-Buffer. Bundling efficiency is slightly increased on average when actin is incubated in G-buffer in the presence of palladin.

TABLE 3.3

T-TEST VALUES FOR G-BUFFER BUNDLING ASSAYS

Ref. #	Comparison	T-Test
	F-Buffer vs. Co-Polymerization Assays in G-Buffer	
21	Ig3, 5 μM	0.009
22	Ig3, 10 μM	0.002
23	Ig3, 20 μM	0.005
24	Ig3L, 5 μM	0.562
25	Ig3L, 10 μM	0.050
26	Ig3L, 20 μM	0.019
27	Ig3L P, 5 μM	0.069
28	Ig3L P, 10 μM	0.737
29	Ig3L P, 20 μM	0.140
30	Ig34, 5 μM	0.659
31	Ig34, 10 μM	0.147
32	Ig34, 20 μM	0.003
33	Ig34 P, 5 μM	0.171
34	Ig34 P, 10 μM	0.010
35	Ig34 P, 20 μM	0.812

3.3.2 Fluorescence Microscopy

In order to visualize the F-actin bundles being formed by palladin, we initially carried out fluorescence microscopy imaging studies. These imaging studies showed G-actin being polymerized by palladin and similar bundles being formed under both non-polymerizing and polymerizing conditions by Ig3, Ig3L, and Ig34.

Ig3 was co-incubated with 10 μM of G or F-actin at 0, 5, 10, and 20 μM concentrations under non-polymerizing (G-buffer) and polymerizing (F-buffer) conditions as described in the experimental section under G and F-buffer Fluorescence Microscopy. After dilution and staining with phalloidin, filaments were present and bundled under G-buffer conditions as shown in Figure 3.14. Under F-buffer conditions, the background of F-actin filaments was cleared and bundles formed when palladin was present.

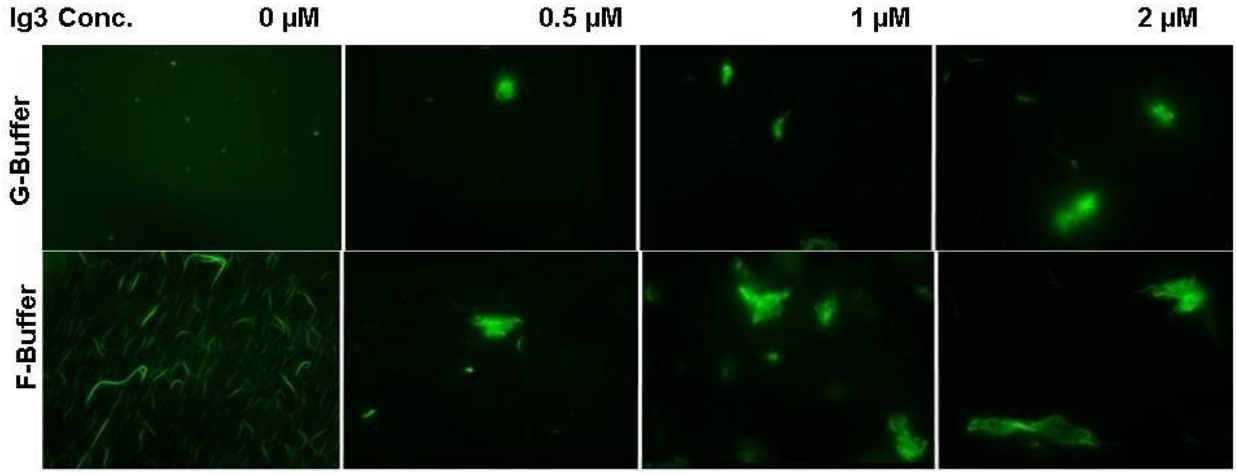

Figure 3.14. Fluorescence Microscopy Imaging of Actin Bundled by Co-Polymerization with Ig3. 1µM actin was incubated with increasing amounts of the Ig3 domain of palladin in both F-Buffer and G-Buffer. Polymerization along with bundling is visualized in samples with Ig3.

These assays were done with Ig3L as well to visualize G-actin polymerization by the construct. Ig3L was co-incubated with 10 µM of G or F-actin at 0, 5, 10, and 20 µM concentrations under non-polymerizing or polymerizing conditions as described in the experimental section. After dilution and staining with phalloidin, filaments were present and bundled under G-buffer conditions as shown in Figure 3.15. The background of F-actin filaments was cleared when palladin was present during F-buffer conditions. The Ig3L bundling may have been to a greater extent than the Ig3 assays as evident by the larger bundles formed.

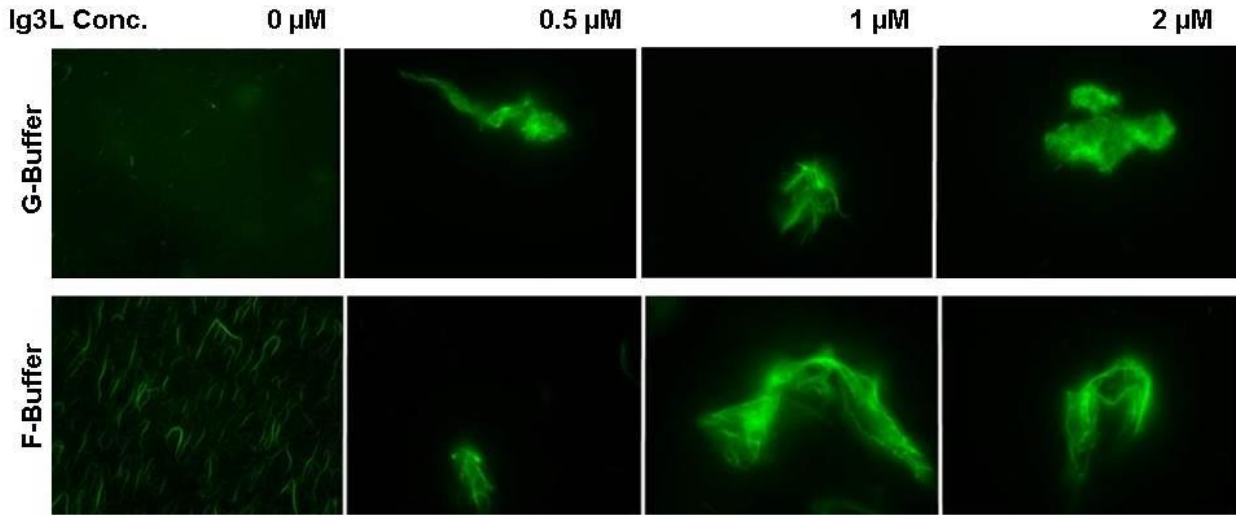

Figure 3.15. Fluorescence Microscopy Imaging of G-Actin Bundled by Co-Polymerization with Ig3L. 1µM actin was incubated with increasing amounts of the Ig3 domain of palladin in both F-Buffer and G-Buffer. Polymerization along with bundling is visualized in samples with Ig3L.

Palladin domains Ig3, Ig3L, and Ig34 were incubated with 10 µM F-actin at 0, 5, 10, and 20 µM concentrations. Upon dilution and phalloidin staining, similar bundling was observed throughout all samples as seen in Figure 3.16. The background of actin filaments was cleared in these samples though the extent of bundling was unable to be quantified.

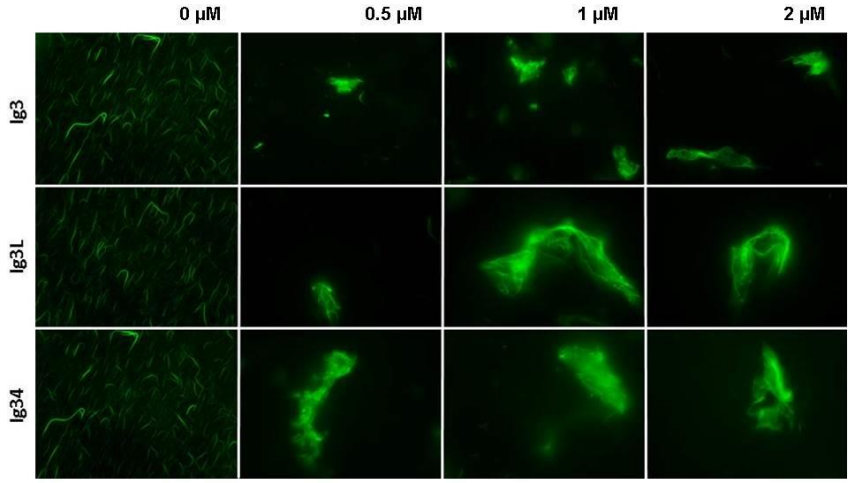

Figure 3.16. Fluorescence Microscopy Imaging of Actin Bundled with Palladin Domains. 1µM actin was incubated with increasing amounts of the Ig3, Ig3L, and Ig34 domains of palladin in F-Buffer. Similar bundling is observed among those samples with palladin.

3.3.3 Electron Microscopy

In order to better visualize the F-actin bundles being formed when G-actin is co-polymerized under G-buffer conditions with palladin, transmission electron microscopy experiments were done with Ig34. These images show the bundles that are formed during co-polymerization as being parallel, as opposed to being perpendicularly cross-linked, as described in Figure 1.3. No new branches are formed coming off the bundles

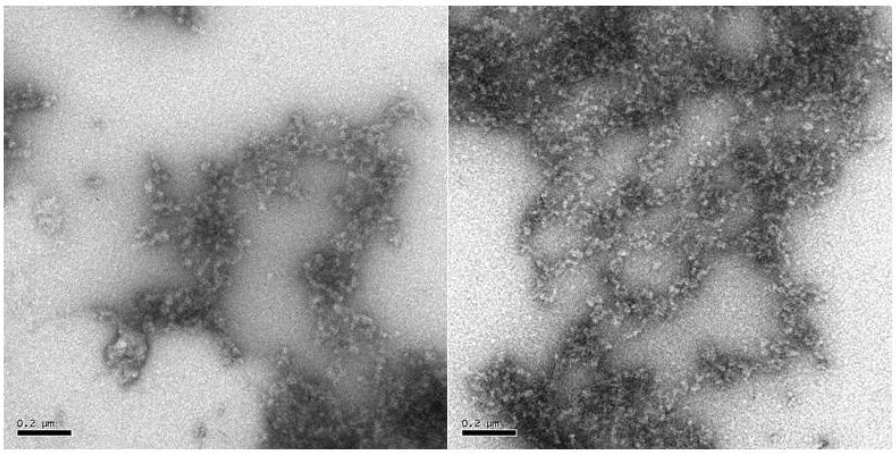

Figure 3.17. Electron Microscopy of G-Actin.

Electron microscopy of G-actin shows no filament formation but simply the monomeric form, shown in Figure 3.17. Figure 3.18 reveals strong parallel bundles being formed that are about 80 nm thick when 20 μM Ig34 is co-polymerized with 3 μM of G-actin under non-polymerizing buffer conditions. Single actin filaments are about 8 nm thick.

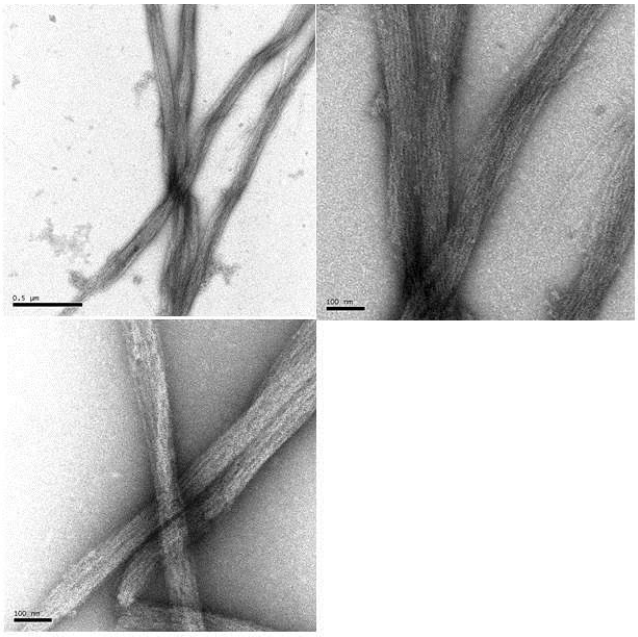

Figure 3.18. Electron Microscopy of G-Actin Co-Polymerized with a High Amount of Palladin. 3μM G-actin was polymerized in G-Buffer in the presence of 20 μM Ig34.

Co-polymerization with a decreased palladin to actin ratio, 10 μM Ig34 and 3 μM G-actin, show bundles with a decreased number of single actin filaments involved, as shown in Figure 3.19.

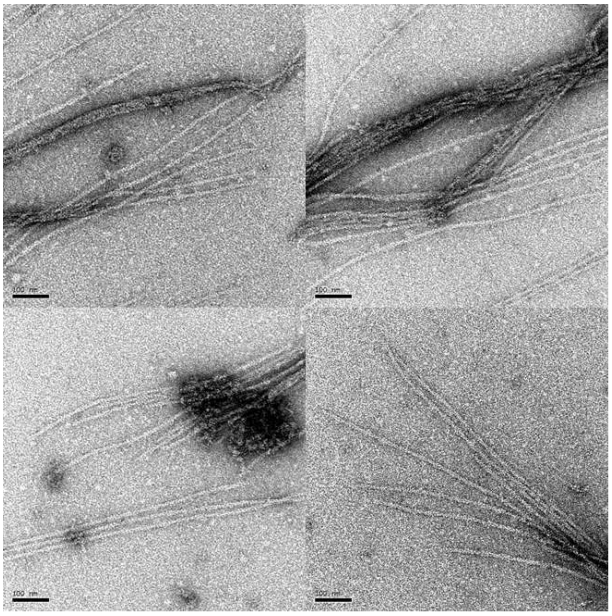

Figure 3.19. Electron Microscopy of G-Actin Co-Polymerized with a Low Amount of Palladin. 3μM G-actin was polymerized in G-Buffer in the presence of 10 μM Ig34.

3.4 Analytical Ultracentrifugation of Palladin

Analytical ultracentrifugation studies were used to determine the oligomeric state of palladin. An initial scan detected aggregation of Ig3 that was prepared without DTT, which is indicated by an increase in absorbance at 400 nm, shown in Figure 3.20, A, by the black line. This sample was used to conduct sedimentation velocity studies but could not be analyzed due to the aggregation. The Ig3 sample with DTT, Ig3L, and Ig34 samples showed no aggregation and could be analyzed.

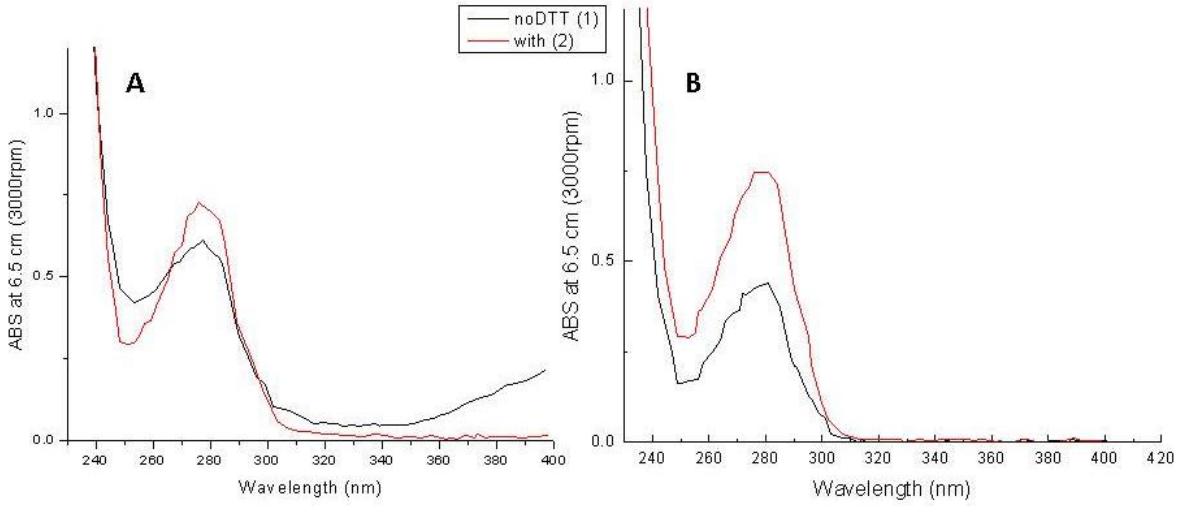

Figure 3.20. Initial Analytical Ultracentrifugation Scan. An initial scan was conducted at 3,000 rpm and 6.5 cm from 230 nm to 400 nm to detect any aggregation and check the total absorbance. A) Ig3 with DTT (red line) shows no aggregates while Ig3 without DTT (black line) shows aggregates at 400 nm. B) Ig3L (black line) and Ig34 (red line) show no aggregation. Both buffers contained DTT.

The sedimentation velocity patterns, shown in Figure 3.21, show classic boundary movement. The boundary of low to high absorbance is initially vertical and progressively becomes broader. The plateau regions also decrease as the protein sample becomes radially diffuse. This rate of movement of the boundary region is then used to determine the rate of movement of the sedimenting protein which in turn leads to the calculation of the sedimentation coefficient, s*.

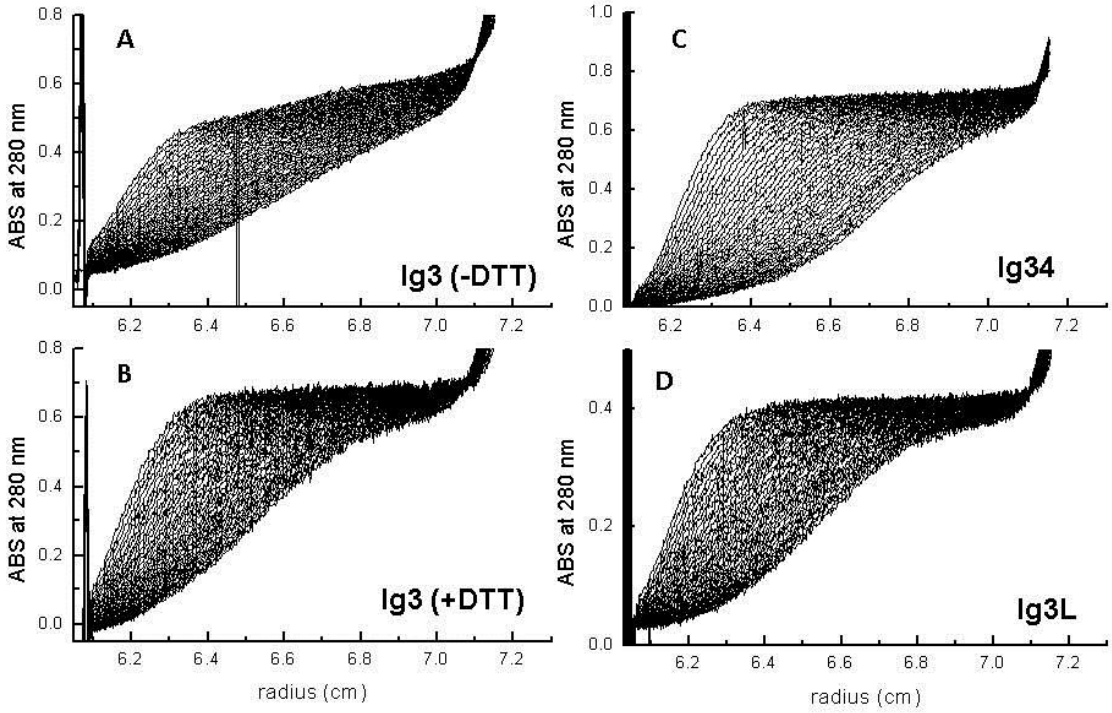

Figure 3.21. Sedimentation Velocity Patterns of Analytical Ultracentrifugation at A_{280}. 40 scans were taken every 6 minutes from 6.1 cm to 7.2 cm radius after 1 hour of centrifugation. Sedimentation patterns of (A) 50 µM Ig3 without DTT, (B) 70 µM Ig3 with DTT, (C) 40 µM Ig34, and (D) 40 µM Ig3L.

Figure 3.22 shows the sedimentation coefficient distributions of Ig3, Ig3L, and Ig34 calculated from the sedimentation velocity experiment. All proteins sediment as monomers in solution. Figure 3.23 then displays a g(s) fit or dc/dt fit gives the S-value and molecular weight values presented in Table 3.4.

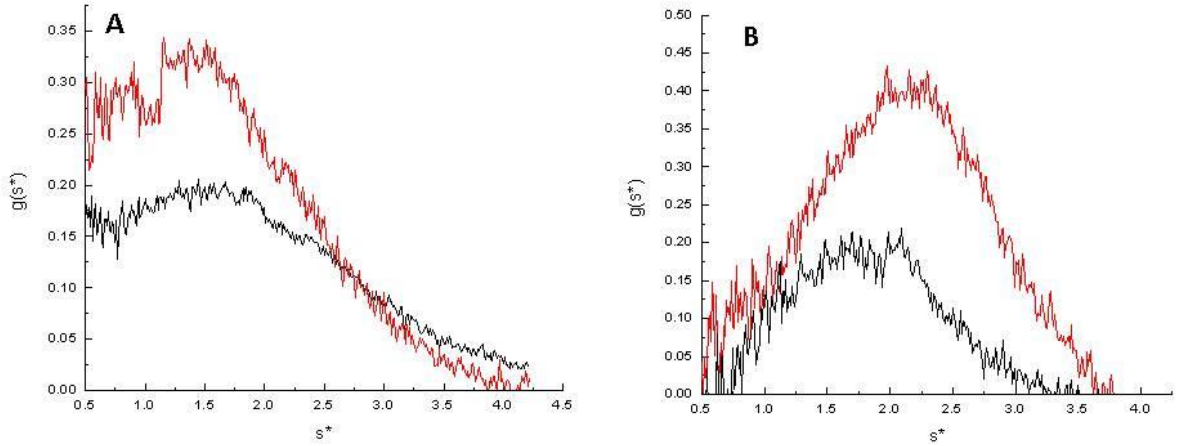

Figure 3.22. Sedimentation Profiles by Analytical Ultracentrifugation. A) Ig3 *g(s*)* profile at 70 µM, with DTT (red line) and at 50 µM without DTT (black line). B) Ig3L *g(s*)* profile at 40 µM (black line) and Ig34 *g(s*)* profile at 40 µM (red line).

TABLE 3.4

AUC CALCULATED SEDIMENTATION VALUES AND MOLECULAR WEIGHTS

Protein	Theoretical MW	AUC Calculated MW	S-Value
Ig3	12.0 kDa	10.7 kDa	1.62
Ig3L	15.0 kDa	16.0 kDa	1.85
Ig34	26.6 kDa	24.1 kDa	2.14

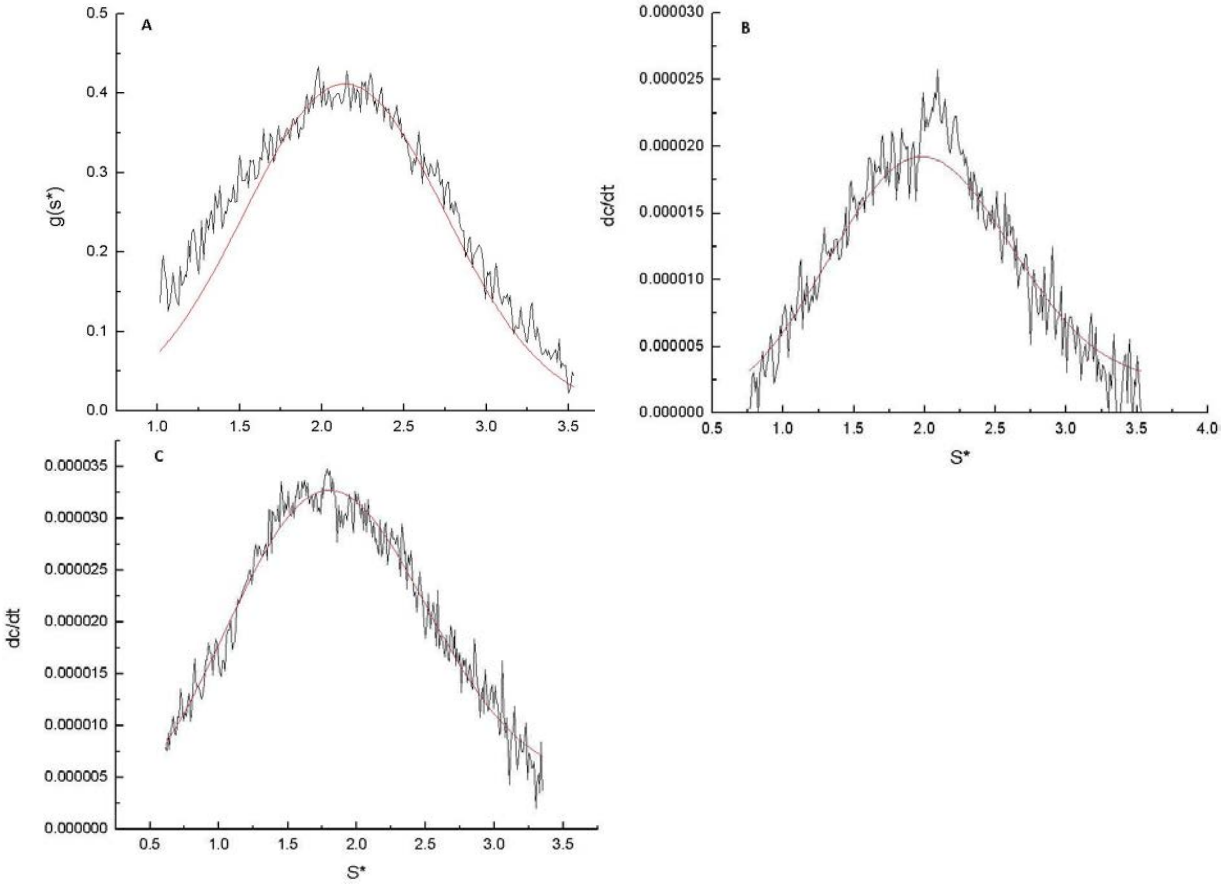

Figure 3.23. Sedimentation Profiles by Analytical Ultracentrifugation with Analyses. A) Ig34 *g(s*)* fit (red line) at 40 µM, B) Ig3L DC/DT+ fit (red line) at 40 µM, and C) Ig3 DC/DT+ fit (red line) at 70 µM, with DTT.

4. DISCUSSION

4.1 The Effects of Phosphorylation on Actin Binding and Bundling by Palladin

Within this thesis, I have worked to increase our knowledge of the interaction of palladin with both F and G-actin, which has been shown to play a critical role in basic cellular processes and cancer metastasis [35-37, 42, 68, 69]. With recent studies showing that Akt1 takes a role in regulating palladin within cells through phosphorylation, it is important to further understand the protein-protein interaction between palladin and F-actin and how the interaction is affected by this post-translational modification [74, 75, 82]. By using *in vitro* assays, we are able to more accurately define the specific interactions between palladin and actin and how the binding, bundling, and polymerization are affected by phosphorylation in the linker region between the Ig3 and Ig4 domains of palladin.

4.1.1 The Binding of Actin by Palladin

To study the binding interaction between palladin and actin, we utilized a binding co-sedimentation assay under a standard set of conditions, *in vitro.* By holding the concentration of F-actin constant and titrating in a saturating amount of palladin, we were able to compare dissociation constants of our palladin constructs and their phosphomimetic partners. The binding studies of the Ig domains Ig3, Ig3L, and Ig34 resulted in dissociation constants in the range of previous studies of palladin and are summarized in Table 3.1 [38]. These studies had been carried out previously but were repeated here to allow us to compare our wild type and phosphomimetic constructs and to obtain values for Ig3L, which are unpublished. Also, our data analysis was different, as we used a method to standardize our raw data as described in the experimental section. The dissociation constants are also similar to other actin-binding proteins

studied, which are in the 1-10 μM range [90, 91]. Our values obtained for Ig34 are a lower dissociation constant, i.e. a greater binding affinity, than obtained previously but what is important here is the comparison in standard conditions among the various constructs.

When we compare these five constructs, we see that the Ig34 domain and its phosphomimetic bind more tightly than Ig3, Ig3L, or Ig3L P. While Ig34 and Ig34 P may bind with greater affinity than these other constructs, little appreciable difference exists between the wild type (Ig3L and Ig34) and their respective phosphomimetic forms. This suggests that the phosphorylation of palladin does not increase its binding affinity for F-actin. This fact will be important in section 4.1.3 when the effects of phosphorylation on palladin and actin bundling are discussed more thoroughly.

We utilized the co-sedimentation assay because other binding assays are simply not as effective when working with actin. Actin poses a unique problem because of its inherent ability to polymerize from the monomer to polymer form. Other assays, like native gel electrophoresis were attempted but relevant data could not be obtained because of the polymerization of actin by palladin, as discussed in section 4.2. Direct assays like gel filtration or equilibrium dialysis would be complicated by the size of F-actin. Indirect methods of observing binding like NMR, CD, ITC, and fluorescence are complicated for the same reason. As discussed in the introduction, the mechanism behind this polymerization is through the charged surface of actin. Its highly charged surface is one of the reasons so many diverse proteins are capable of binding actin, but it quickly complicates the description of the binding interaction as there are no consensus actin-binding motifs and no respective site on actin which proteins bind to either. Without such a "lock and key" model for actin and palladin, describing the binding site interaction proves difficult. With this in mind, one could reduce the interaction of full length palladin to a charge-charge

interaction but in light of the fact that it can saturate actin in the low μM range indicates that specific interactions are also occurring.

We observed a slight difference in actin binding between Ig3 and Ig3L. This indicates that specific binding interactions only occur between the Ig3 domain and actin and that the addition of the linker region may slightly increase binding affinity, as linker is incapable of binding F-actin [38]. The addition of the Ig4 domain to Ig3L, as a tandem single construct, increases the actin binding affinity by an appreciable amount, indicating that either binding by Ig4 is activated when joined to Ig3 through the linker region or that Ig4 enhances the actin binding affinity of Ig3. Although this latter hypothesis is plausible, the bundling data discussed in 4.1.2 suggests that this model is problematic because of the size constraints of filamentous actin and other considerations.

Given that phosphorylation does not appear to enhance actin binding, this protein modification probably does not play a role in regulating the direct interaction of palladin with actin. However phosphorylation may influence interactions with other palladin binding partners. Ezrin binds to Ig4 and its role as a cytoskeletal organizer could theoretically be regulated by an altered affinity to palladin, which seemingly acts as a scaffolding and organizing protein [42]. Palladin has other binding partners but they exist in regions outside of Ig34. The binding interaction between these partners and palladin may be changed by phosphorylation, but this is doubtful because of their spatial distance from the modification. Overall, the structural and functional dynamics of Ig34 appear to be much different than the Ig3 and Ig3L domains but its binding to actin does not appear to be altered by phosphorylation.

4.1.2 The Bundling of Actin by Palladin

To study the bundling of F-actin by palladin, we utilized a co-sedimentation assay with both low speed and high speed centrifugation. By holding the concentration of F-actin constant and varying the concentration of palladin, we are able to compare the bundling capabilities of the various Ig domains. With the bundling studies we have shown a single immunoglobulin domain capable of bundling actin. This bundling activity of Ig3 has not been previously reported. Initial studies by Dixon *et al.* described Ig3 as not capable of bundling F-actin, but upon further analysis of that initial raw data, more actin is seen in the bundle than in other non-bundling domains [38]. Our studies with Ig4 have confirmed previous findings that it is not capable of bundling. The presence of both Ig3 and Ig4 in solution, as separate purified constructs, does not increase bundling of actin above what is observed for Ig3 alone. We also showed that Ig3L is more capable of bundling than Ig3. The addition of the linker region may cause a structural change in Ig3, allowing it to more effectively bundle. The addition of the linker region does cause a slight increase in binding affinity, which may indicate it causes this change allowing Ig3 to bind tighter. The linker region likely does not contribute to bundling directly, as previous studies show the linker region incapable of bundling [38]. When Ig4 is incubated in a bundling assay along with Ig3L, there is again no increase over Ig3L alone. As in the previous study, Ig34 was shown to be most capable of bundling F-actin. Existing as the entire Ig34 domain may cause a conformational change in Ig4, which then allows Ig4 to bind and bundle actin, or the presence of Ig4 allows the linker or Ig3 to more effectively bundle actin.

The two models set forth, depicted in Figure 4.1, are the enhancement of bundling through Ig3 or the “activation” of Ig4, could be the reason for the increase in bundling over Ig3 and Ig3L. The dissociation constant of Ig3L is slightly greater than that of Ig3, indicating that

Ig3L may have a higher affinity for F-actin. Ig3L has a higher dissociation constant than Ig34 and thus can not bind actin as tightly. If Ig4 increases the binding affinity, then we can reduce the cause of the increase to the two domains and eliminate the linker region as a contributing factor in bundling. The linker may aid bundling by affecting Ig3, but does not appear to participate directly, as evident from the binding studies and previous data [38]. Sequentially, bundling of F-actin is increased by addition of the linker to Ig3, addition of Ig4 to Ig3L, and phosphorylation of Ig34, as seen in the bundling data. These increases in bundling capacity could be reduced to structural effects of these changes on the Ig3 domain alone. Also, considering the increases in binding affinity and bundling efficiency with the addition of the Ig4 domain, it is possible that Ig4 undergoes a conformational change allowing it to be capable of binding and bundling actin. These two models, Ig3 bundling increase or activation of Ig4, could explain the sequential increase in bundling upon addition of the linker, Ig4, and phosphorylation. This is depicted in Figure 4.1. The only way to determine whether a change in Ig3 or Ig4 occurs is to carry out structural studies on the various regions.

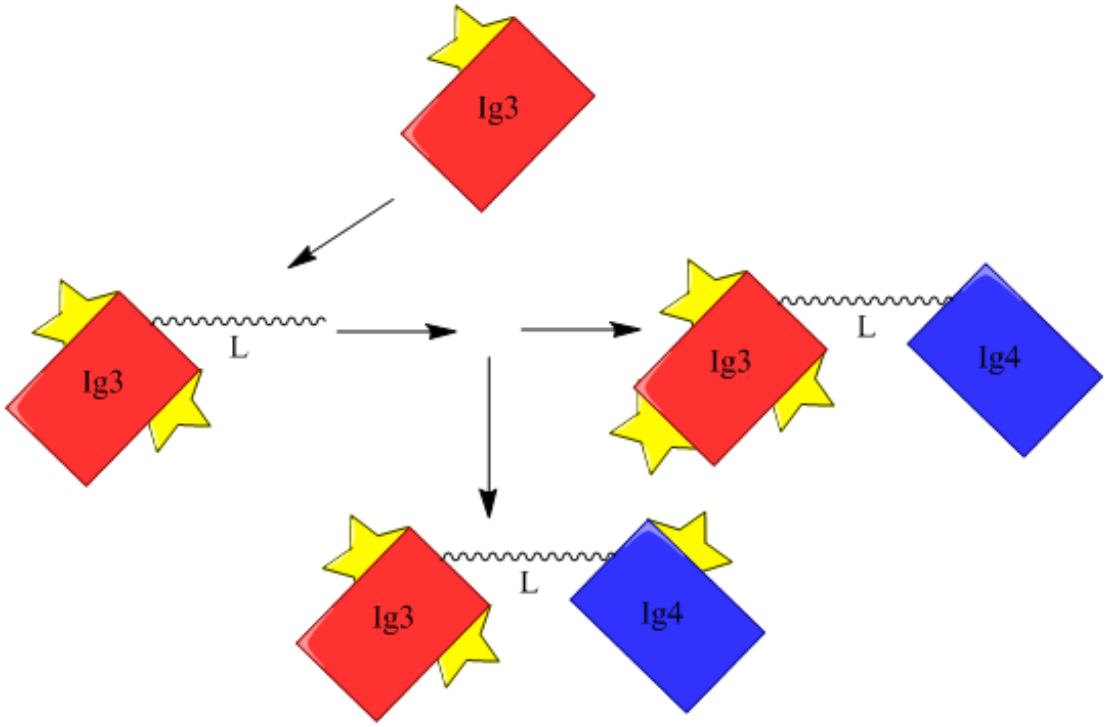

Figure 4.1 Sequential Increase in Bundling by Various Palladin Constructs. Yellow stars indicate bundling capacity and location the increase takes place. More stars indicate greater bundling capacity. The addition of linker causes a slight increase in affinity and allows Ig3 to bundle more effectively. The addition of Ig4 to Ig3L then allows Ig3 to further bundle more effectively or is made capable of binding and thus bundling F-actin.

Another possibility for the cause in the Ig34 bundling capacity increase is in dimerization through Ig4. Our analytical ultracentrifugation studies showed no constructs exist as dimers in solution. It is possible though that Ig4 is capable of binding F-actin when it is expressed as a whole Ig34 domain and bound to F-actin. This has been shown to occur in the vinculin tail domain [92]. In short, F-actin was shown to induce or stabilize a conformational change in the vinculin tail domain, allowing it to dimerize on itself. This is a possibility but would be difficult to study through most methods. Future electron microscopy and/or chemical crosslinking of the Ig34 domain in the presence of F-actin may provide some insights into this possibility.

Our studies with the separate Ig3 and Ig4 constructs as well as the Ig3L and Ig4 constructs in the bundling assay show that the two domains must be one tandem construct, as in Ig34, to provide an increase in bundling capacity. Compared to the studies with just Ig3 or Ig3L in solution, the data indicated that there was no difference between them. What this tells us is that being one tandem construct (Ig3-Linker-Ig4) creates some change in the domains not present if the two domains are mixed in solution together. Six of the seven palladin isoforms are expressed with the Ig34 domain and variations of the polyproline region and N-terminal Ig domains. While binding and bundling of actin by all of these isoforms may not be different, our data indicates that variations of domains around the Ig3 and Ig4 regions have a considerable effect on actin binding and bundling. Palladin has roles as both an actin cytoskeleton regulator and scaffolding protein, therefore the various isoforms may be expressed in the various tissues to maintain different types of actin structures.

4.1.3 The Increase in Bundling of Actin after Phosphorylation of Palladin

The addition of the phosphate moiety to Ig3L and Ig34, modeled in this research by the use of a glutamic acid phosphomimetic mutation, lends some more information to not only our questions about the effect of phosphorylation on palladin but also sheds light on how palladin functions in general. In the Ig3L and Ig3L P studies, we observed that the phosphomimetic mutation did not alter binding or bundling. Similarly, the phosphomimetic did not increase the Ig34 binding affinity for F-actin. When the bundling assay was carried out, an increase in bundling at lower concentrations was observed, which indicated phosphorylation aids the Ig34 domain bundling efficiency.

The phosphomimetic constructs were not able to bind F-actin more efficiently or bind more tightly, indicating that a change in the charge of the linker region is not involved in the

interaction. This is to say that the phosphate changes the charge-profile of the linker region, bringing the overall charge closer to that of F-actin. If the interaction of palladin and actin were based solely on electrostatics, then the addition of such a charged group would likely change the binding interaction. With the previous discussion in 4.1.2 on conformational change in Ig3 or Ig4 and the fact that our studies indicate that a change in charge does not affect binding affinity, it is reasonable to extend this theory to suggest that a conformational change of Ig3 or Ig4 may explain how the phosphorylation causes a change in bundling abilities. With the addition of the phosphate group, the flexibility of the linker or position of the two domains with respect to each other may change spatially. Alternatively Ig34 may undergo some conformational change, enabling the Ig3 and Ig4 domains to bundle F-actin more efficiently. These three possibilities are drawn in Figure 4.2. Myosin-binding protein C is an example of phosphorylation in the linker region of an actin-binding protein in which the protein being phosphorylated undergoes a change in actin binding properties, though these are attributed to electrostatics changes [53, 93]. Conformational change in a protein caused by phosphorylation in a linker region has been described in CheB, OmpR, and p85 proteins [94-96]. These studies showed that phosphorylation in a linker region altered the function and structure of these proteins.

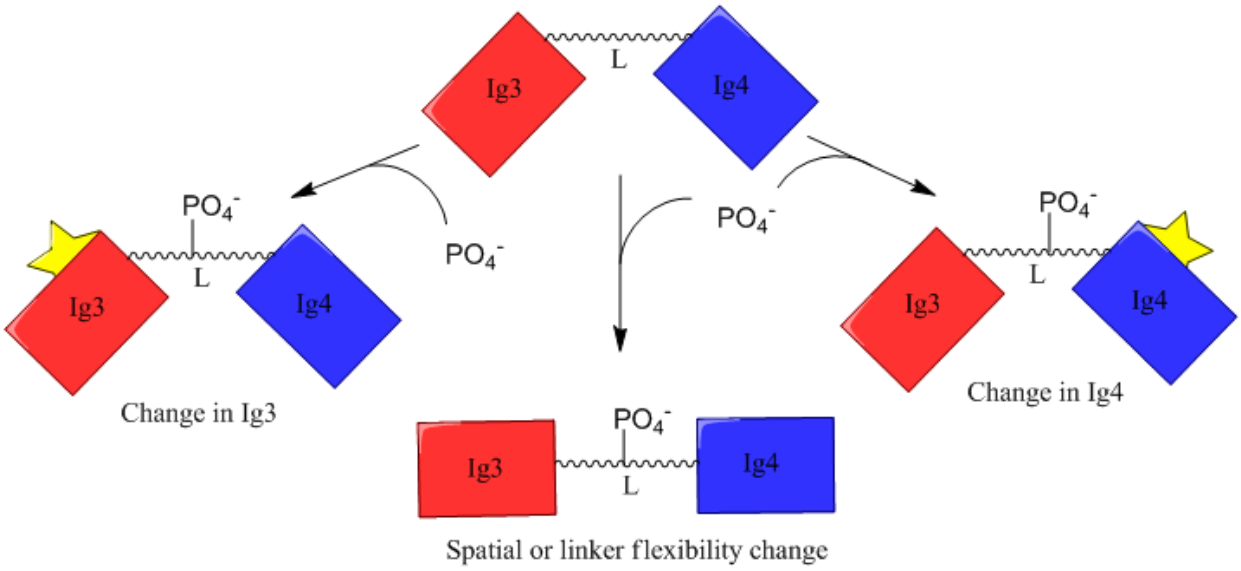

Figure 4.2 Theoretical Changes in Ig34 Upon Phosphorylation Leading to Increased F-actin Bundling

If we compare the Ig3L and Ig34 wild type and phosphomimetic bundling data, we see more clues as to the importance of Ig4 and its role in palladin. Although the phosphomimetic Ig3L does not bundle F-actin with any greater efficiency than the wild type Ig3L, we did observe a significant difference between the Ig34 wild type and phosphomimetic bundling. This suggests that the Ig4 domain plays a role in the bundling of F-actin that is influenced by the phosphorylated status of the linker region. The phosphorylation likely works though changing the overall Ig34 structure or the flexibility/orientation of two domains with respect to each other, which would mean that Ig4 is binding and aiding in the bundling of F-actin. These conclusions will be investigated in future structural studies.

These findings imply that structural regulation of palladin, or lack thereof, is involved in cancer cell metastasis. While overproduction of palladin has been implicated as the structural cause of cancer cell metastasis in numerous studies, there is most likely an element of structural regulation as well [41, 71-73]. Studies which contrast these show that decreased production of palladin leads to cell migration [74, 75, 82]. These studies are at odds with each other in their

description of the role of palladin in cancer cell migration, but this controversy is reconciled by a discussion in the Chin and Toker study of the possibility of different migration assays and chemoattractants being used in the Goicoechea *et al.* paper versus their own work [71, 74]. Previous work shows palladin expression levels changing actin bundles *in vivo* and that the overexpression causes increased motility. Therefore, it is likely that a connection exists between phosphorylation levels of palladin, its expression level, and cell motility [37]. Chin and Toker's work shows that a palladin construct that can not be phosphorylated at serine 507 does not inhibit cell motility, while phosphorylated palladin can inhibit this activity [74]. If this is the case, then invasive cell motility caused by palladin overexpression may be reversed by Akt1 phosphorylation. Our research shows that the phosphomimetic palladin is capable of bundling twice as much F-actin at low concentrations when compared to wild type palladin, as shown in Figure 7. If phosphorylated palladin bundles more F-actin as well as causes decreased cell migration as shown by Chin and Toker, then there may be a point at which bundles in invadopodia and podosomes inhibit rather than help these cellular structures and their function.

4.2 Co-Polymerization of G-Actin with Palladin

From initial studies done in lab, we found that palladin was capable of polymerizing G-actin to F-actin under non-polymerizing, low ionic strength conditions. While G-actin requires the presence of divalent cations in order to reduce the net-negative charge and repulsion among the monomeric form, these studies were done in the absence of potassium and magnesium. These studies carried out with Ig3, Ig3L, and Ig34 indicate that they all polymerize the majority of G-actin present in solution. This polymerization in the presence of palladin suggests that palladin is capable of binding monomeric actin or may cause G-actin to nucleate to a trimer before it starts

polymerizing. Not only does palladin cause polymerization, but the resulting filaments are more crosslinked when co-polymerized with the Ig3 and Ig3L domains.

In the case of Ig3, the domain is able to more efficiently bring together separate filaments as they are polymerizing instead of after they have formed. This could be due to Ig3's lower affinity and F-actin bundling capacity. If Ig3 is not as capable at bringing together pre-formed filaments as Ig3L or Ig34, then co-polymerization may allow the chance to associate with filaments as they are being formed and bundle with greater efficiency. This same bundling efficiency is reached by Ig3L and Ig34 at lower concentrations and when filaments are pre-formed. Since the binding efficiency of Ig3L and Ig34 are nearly double that of Ig3, it indicates that less Ig3L or Ig34 is required to bundle the same amount of actin. The co-polymerization assays then show that ability of palladin to bundle F-actin may depend on whether or not actin is polymerized when they associate. This adds another layer of complexity to the relationship between actin and palladin. Actin polymerization has been studied in invadopodia formation and is the driving force behind the elongation of the invadopodia or podosomes cell structure while bundles of F-actin provide structural stability [97, 98]. The role of palladin in invasive cell motility may be more involved than previously thought in light of this new data. Our fluorescence microscopy studies and initial transmission electron microscopy data show that the bundles being formed by palladin when co-polymerized are similar to those when actin is pre-polymerized, but this data is still preliminary. Co-polymerization may or may not create a different actin bundle structure then, such as perpendicular bundles being formed. If similar bundle formations are created under both conditions, then instead of palladin having two separate abilities to create distinct structures based on the oligomeric state of actin, it may be capable of

driving and regulating actin polymerization while maintaining a stable bundle structure within invadopodia.

Furthermore, it does not appear that the wild type and phosphomimetic constructs differ in their ability to bundle actin when filaments are pre-formed or co-polymerization occurs. This indicates that phosphorylation strictly functions as a regulatory post-translational modification capable of increasing bundling efficiency of pre-formed filaments but does not affect polymerization or bundling capacity of actin when actin filament formation is driven by palladin. Our research then shows the specificity of the regulatory ability of phosphorylation of palladin.

4.3 Future Directions

With the work presented in this thesis, we further understand palladin's dynamic interaction with actin. More work will need to be done to understand questions created by this research. Some of these inquiries will deal with structural changes within palladin upon phosphorylation, using true phosphorylation of palladin in place of a phosphomimetic, polymerization of actin by palladin, the structural basis of the interaction between palladin and actin, what role Ig4 plays in the palladin-actin relationship, and the relationship between palladin expression levels and the actin structure inside invadopodia.

NMR structural studies could aid us in observing the difference between the phosphorylated and non-phosphorylated palladin. This would be a matter of finding chemical shift data for the wild type Ig34 and comparing it to the phosphomimetic or a phosphorylated wild type Ig34 domain. With chemical shift assignments already available for Ig3 and Ig4, one could compare these to the chemical shift data for Ig34 and Ig34 P and find what the difference is between the lone domains, the paired Ig34 structure, and the phosphorylated construct. NMR

studies could also show what structural difference occurs in Ig4 when joined to Ig3L. A solution structure could be solved on top of this to obtain the 3-dimensional structural differences.

Studies could also be done to quantify any differences in the phosphomimetic mutants we created and direct phosphorylation by Akt1 at serine 507. This would give us an idea of how accurate using the phosphomimetic model really is. While the accuracy of the model may be slightly off, it is ultimately a more stable and reproducible method for quantifying the difference between wild type and post-translationally modified proteins.

Kinetic studies of polymerization by palladin have already begun in our lab. These studies have focused on Ig3 and some mutants of this domain and quantified the kinetic rates of polymerization. Further work could look at the Ig3L and Ig34 constructs to observe any difference they have on accelerating polymerization or effects on the critical concentration of actin.

To observe the structural basis of the interaction between palladin and actin, electron cryomicroscopy studies will most likely need to be done. Considering the restraints that the filamentous form of actin places on studying structural interaction, high resolution cryo-EM may provide insights into the structural differences between Ig3 and Ig34 bundling F-actin. This images and the 3-dimensional reconstruction could show the binding areas of these domains and how they interact to bundle actin.

Finally, cellular studies could be done to define the relationship between palladin expression levels and the actin structure inside invadopodia. Chin and Toker's work has begun to investigate this correlation, but thorough and comprehensive studies could be done to fully delineate the cytoskeletal structure of invadopodia with regards to palladin. By quantifying the

levels of palladin expression, levels of phosphorylation, and differences in actin cytoskeletal structure, the relationship between palladin and invadopodia could be better understood.

5. CONCLUSIONS

The research discussed in this thesis further describes the interaction of palladin and actin, proteins critical for cancer cell metastasis. The Ig3 domain of palladin was found to be the smallest unit of palladin necessary for F-actin bundling, previously thought to require both Ig3 and Ig4 domains. This domain was also found to polymerize and bundle actin with greater efficiency when it was allowed to co-polymerize with G-actin compared to F-actin filament bundling. We found that increasing the size of the construct from Ig3 to Ig3L to Ig34 increased the bundling of F-actin and that the addition of the Ig4 domain to Ig3L increased binding affinity and bundling efficiency. We confirmed and quantified the bundling difference of actin by Ig34 and its phosphorylated structure using a phosphomimetic model.

These results allow us to make a number of conclusions about the structural basis of the actin-palladin interaction. First, the attachment of Ig4 to Ig3L likely causes a structural change within Ig4, allowing it to contribute to actin binding and bundling by palladin. With the knowledge that Ig4 is a player in the actin-palladin interaction, we can extrapolate this idea to the phosphorylation of the linker region. The phosphorylation of palladin likely causes a structural change in Ig34, which allows it to more efficiently bundle F-actin. This structural change will be studied in the future using structural methods.

Our results also describe how palladin influences polymerization of G-actin and bundling of the filaments after polymerization. This data lends more evidence to studies describing the role of palladin in metastatic cancer, except now the added dimension of actin polymerizing is added to palladin's abilities. Actin polymerization is the underpinning mechanism of a cell podosomes, as actin polymerizes to drive a projection forward. Along with bundles that

maintain the shape and strength of podosomes or invadopodia, actin must be regulated in a number of ways to enable its movement. By describing the interaction of palladin and actin more thoroughly, we can understand the role of palladin in the regulation of the actin-based structures of cancer cell metastasis.

REFERENCES

REFERENCES

1. Nelson, D.L., Cox, Michael M., *Principles of Biochemistry,* Fifth ed2008, New York: W.H. Freeman and Company.

2. Straub, B.F., *Studies from the Institute of Medical Chemistry, University of Szeged*, S.-G.A. (Szeged), Editor 1942, Karger.

3. Elzinga, M., et al., *Complete amino-acid sequence of actin of rabbit skeletal muscle.* Proc Natl Acad Sci U S A, 1973. **70**(9): p. 2687-91.

4. Martonosii, A., C.M. Molino, and J. Gergely, *THE BINDING OF DIVALENT CATIONS TO ACTIN.* J Biol Chem, 1964. **239**: p. 1057-64.

5. Straub, F.B. and G. Feuer, *[Adenosine triphosphate, the functional group of actin].* Kiserl Orvostud, 1950. **2**(2): p. 141-51.

6. Kabsch, W., et al., *Atomic structure of the actin:DNase I complex.* Nature, 1990. **347**(6288): p. 37-44.

7. Elzinga, M. and J.H. Collins, *The primary structure of actin from rabbit skeletal muscle. Five cyanogen bromide peptides, including the NH2 and COOH termini.* J Biol Chem, 1975. **250**(15): p. 5897-905.

8. Alberts, B.B., Dennis. Lewis, Julian. Raff, Martin. Roberts, Keith. Watson, James D., *Molecular Biology of the Cell*. Third ed1994, New York: Garland Publishing.

9. Schrödinger, L., *The PyMOL Molecular Graphics System*.

10. Holmes, K.C., et al., *Atomic model of the actin filament.* Nature, 1990. **347**(6288): p. 44-9.

11. Fujii, T., et al., *Direct visualization of secondary structures of F-actin by electron cryomicroscopy.* Nature, 2010. **467**(7316): p. 724-8.

12. Pantaloni, D., et al., *A model for actin polymerization and the kinetic effects of ATP hydrolysis.* Proc Natl Acad Sci U S A, 1985. **82**(21): p. 7207-11.

13. Cooper, G.M., Hausman, Robert E., *The Cell: A Molecular Approach*. Fifth ed2009, Washington, D.C.: ASM Press.

14. Pardee, J.D. and J.A. Spudich, *Mechanism of K+-induced actin assembly.* J Cell Biol, 1982. **93**(3): p. 648-54.

15. Ohm, T. and A. Wegner, *Mechanism of ATP hydrolysis by polymeric actin.* Biochim Biophys Acta, 1994. **1208**(1): p. 8-14.

16. Pieper, U. and A. Wegner, *The end of a polymerizing actin filament contains numerous ATP-subunit segments that are disconnected by ADP-subunits resulting from ATP hydrolysis.* Biochemistry, 1996. **35**(14): p. 4396-402.

17. Carlier, M.F., D. Pantaloni, and E.D. Korn, *The mechanisms of ATP hydrolysis accompanying the polymerization of Mg-actin and Ca-actin.* J Biol Chem, 1987. **262**(7): p. 3052-9.

18. Pfaendtner, J., et al., *Nucleotide-dependent conformational states of actin.* Proc Natl Acad Sci U S A, 2009. **106**(31): p. 12723-8.

19. Ayscough, K.R., *In vivo functions of actin-binding proteins.* Curr Opin Cell Biol, 1998. **10**(1): p. 102-11.

20. Heidemann, S.R., et al., *Direct observations of the mechanical behaviors of the cytoskeleton in living fibroblasts.* J Cell Biol, 1999. **145**(1): p. 109-22.

21. Heidemann, S.R. and D. Wirtz, *Towards a regional approach to cell mechanics.* Trends Cell Biol, 2004. **14**(4): p. 160-6.

22. Welch, M.D., et al., *Actin dynamics in vivo.* Curr Opin Cell Biol, 1997. **9**(1): p. 54-61.

23. Fedorov, A.A., et al., *The molecular basis for allergen cross-reactivity: crystal structure and IgE-epitope mapping of birch pollen profilin.* Structure, 1997. **5**(1): p. 33-45.

24. Pollard, T.D. and J.A. Cooper, *Actin and Actin-Binding Proteins. A Critical Evaluation of Mechanisms and Functions.* Annual Review of Biochemistry, 1986. **55**(1): p. 987-1035.

25. Vincent, C., T.A. Siddiqui, and L.C. Schlichter, *Podosomes in migrating microglia: components and matrix degradation.* J Neuroinflammation, 2012. **9**: p. 190.

26. Davies, W.A. and T.P. Stossel, *Peripheral hyaline blebs (podosomes) of macrophages.* J Cell Biol, 1977. **75**(3): p. 941-55.

27. Burns, S., et al., *Configuration of human dendritic cell cytoskeleton by Rho GTPases, the WAS protein, and differentiation.* Blood, 2001. **98**(4): p. 1142-9.

28. Chellaiah, M., et al., *Gelsolin deficiency blocks podosome assembly and produces increased bone mass and strength.* J Cell Biol, 2000. **148**(4): p. 665-78.

29. Burgstaller, G. and M. Gimona, *Podosome-mediated matrix resorption and cell motility in vascular smooth muscle cells.* Am J Physiol Heart Circ Physiol, 2005. **288**(6): p. H3001-5.

30. Weaver, A.M., *Invadopodia: specialized cell structures for cancer invasion.* Clin Exp Metastasis, 2006. **23**(2): p. 97-105.

31. Murphy, D.A. and S.A. Courtneidge, *The 'ins' and 'outs' of podosomes and invadopodia: characteristics, formation and function.* Nat Rev Mol Cell Biol, 2011. **12**(7): p. 413-26.

32. Gavazzi, I., M.V. Nermut, and P.C. Marchisio, *Ultrastructure and gold-immunolabelling of cell-substratum adhesions (podosomes) in RSV-transformed BHK cells.* J Cell Sci, 1989. **94 (Pt 1)**: p. 85-99.

33. Linder, S. and P. Kopp, *Podosomes at a glance.* J Cell Sci, 2005. **118**(Pt 10): p. 2079-82.

34. Lu, P., V.M. Weaver, and Z. Werb, *The extracellular matrix: a dynamic niche in cancer progression.* J Cell Biol, 2012. **196**(4): p. 395-406.

35. Parast, M.M. and C.A. Otey, *Characterization of palladin, a novel protein localized to stress fibers and cell adhesions.* J Cell Biol, 2000. **150**(3): p. 643-56.

36. Goicoechea, S., et al., *Palladin binds to Eps8 and enhances the formation of dorsal ruffles and podosomes in vascular smooth muscle cells.* J Cell Sci, 2006. **119**(Pt 16): p. 3316-24.

37. Boukhelifa, M., et al., *A critical role for palladin in astrocyte morphology and response to injury.* Mol Cell Neurosci, 2003. **23**(4): p. 661-8.

38. Dixon, R.D., et al., *Palladin is an actin cross-linking protein that uses immunoglobulin-like domains to bind filamentous actin.* J Biol Chem, 2008. **283**(10): p. 6222-31.

39. Rachlin, A.S. and C.A. Otey, *Identification of palladin isoforms and characterization of an isoform-specific interaction between Lasp-1 and palladin.* J Cell Sci, 2006. **119**(Pt 6): p. 995-1004.

40. Otey, C.A., et al., *Cytoplasmic Ig-domain proteins: cytoskeletal regulators with a role in human disease.* Cell Motil Cytoskeleton, 2009. **66**(8): p. 618-34.

41. Goicoechea, S.M., et al., *Isoform-specific upregulation of palladin in human and murine pancreas tumors.* PLoS One, 2010. **5**(4): p. e10347.

42. Mykkanen, O.M., et al., *Characterization of human palladin, a microfilament-associated protein.* Mol Biol Cell, 2001. **12**(10): p. 3060-73.

43. Einheber, S. and D.A. Fischman, *Isolation and characterization of a cDNA clone encoding avian skeletal muscle C-protein: an intracellular member of the immunoglobulin superfamily.* Proc Natl Acad Sci U S A, 1990. **87**(6): p. 2157-61.

44. Vaughan, K.T., et al., *Molecular cloning of chicken myosin-binding protein (MyBP) H (86-kDa protein) reveals extensive homology with MyBP-C (C-protein) with conserved immunoglobulin C2 and fibronectin type III motifs.* J Biol Chem, 1993. **268**(5): p. 3670-6.

45. Noguchi, J., et al., *Complete primary structure and tissue expression of chicken pectoralis M-protein.* J Biol Chem, 1992. **267**(28): p. 20302-10.

46. Labeit, S., et al., *A regular pattern of two types of 100-residue motif in the sequence of titin.* Nature, 1990. **345**(6272): p. 273-6.

47. Salmikangas, P., et al., *Myotilin, a novel sarcomeric protein with two Ig-like domains, is encoded by a candidate gene for limb-girdle muscular dystrophy.* Hum Mol Genet, 1999. **8**(7): p. 1329-36.

48. Jin, L., et al., *The actin associated protein palladin is important for the early smooth muscle cell differentiation.* PLoS One, 2010. **5**(9): p. e12823.

49. Price, C.J. and N.P. Brindle, *Vasodilator-stimulated phosphoprotein is involved in stress-fiber and membrane ruffle formation in endothelial cells.* Arterioscler Thromb Vasc Biol, 2000. **20**(9): p. 2051-6.

50. Alyonycheva, T.N., et al., *Isoform-specific interaction of the myosin-binding proteins (MyBPs) with skeletal and cardiac myosin is a property of the C-terminal immunoglobulin domain.* J Biol Chem, 1997. **272**(33): p. 20866-72.

51. Freiburg, A. and M. Gautel, *A molecular map of the interactions between titin and myosin-binding protein C. Implications for sarcomeric assembly in familial hypertrophic cardiomyopathy.* Eur J Biochem, 1996. **235**(1-2): p. 317-23.

52. Moolman-Smook, J., et al., *Identification of novel interactions between domains of Myosin binding protein-C that are modulated by hypertrophic cardiomyopathy missense mutations.* Circ Res, 2002. **91**(8): p. 704-11.

53. Shaffer, J.F., R.W. Kensler, and S.P. Harris, *The myosin-binding protein C motif binds to F-actin in a phosphorylation-sensitive manner.* J Biol Chem, 2009. **284**(18): p. 12318-27.

54. Nagy, A., et al., *Differential actin binding along the PEVK domain of skeletal muscle titin.* J Cell Sci, 2004. **117**(Pt 24): p. 5781-9.

55. Bang, M.L., et al., *Myopalladin, a novel 145-kilodalton sarcomeric protein with multiple roles in Z-disc and I-band protein assemblies.* J Cell Biol, 2001. **153**(2): p. 413-27.

56. Duboscq-Bidot, L., et al., *Mutations in the Z-band protein myopalladin gene and idiopathic dilated cardiomyopathy.* Cardiovasc Res, 2008. **77**(1): p. 118-25.

57. Salmikangas, P., et al., *Myotilin, the limb-girdle muscular dystrophy 1A (LGMD1A) protein, cross-links actin filaments and controls sarcomere assembly.* Hum Mol Genet, 2003. **12**(2): p. 189-203.

58. Ruskamo, S. and J. Ylanne, *Structure of the human filamin A actin-binding domain.* Acta Crystallogr D Biol Crystallogr, 2009. **65**(Pt 11): p. 1217-21.

59. Nakamura, F., et al., *Structural basis of filamin A functions.* J Cell Biol, 2007. **179**(5): p. 1011-25.

60. Dominguez, R. and K.C. Holmes, *Actin structure and function.* Annu Rev Biophys, 2011. **40**: p. 169-86.

61. Lee, S.H. and R. Dominguez, *Regulation of actin cytoskeleton dynamics in cells.* Mol Cells, 2010. **29**(4): p. 311-25.

62. Algrain, M., et al., *Ezrin contains cytoskeleton and membrane binding domains accounting for its proposed role as a membrane-cytoskeletal linker.* J Cell Biol, 1993. **120**(1): p. 129-39.

63. Berryman, M., R. Gary, and A. Bretscher, *Ezrin oligomers are major cytoskeletal components of placental microvilli: a proposal for their involvement in cortical morphogenesis.* J Cell Biol, 1995. **131**(5): p. 1231-42.

64. Mouilleron, S., et al., *Structure of a pentavalent G-actin*MRTF-A complex reveals how G-actin controls nucleocytoplasmic shuttling of a transcriptional coactivator.* Sci Signal, 2011. **4**(177): p. ra40.

65. Du, K.L., et al., *Megakaryoblastic leukemia factor-1 transduces cytoskeletal signals and induces smooth muscle cell differentiation from undifferentiated embryonic stem cells.* J Biol Chem, 2004. **279**(17): p. 17578-86.

66. Offenhauser, N., et al., *The eps8 family of proteins links growth factor stimulation to actin reorganization generating functional redundancy in the Ras/Rac pathway.* Mol Biol Cell, 2004. **15**(1): p. 91-8.

67. Fazioli, F., et al., *Eps8, a substrate for the epidermal growth factor receptor kinase, enhances EGF-dependent mitogenic signals.* EMBO J, 1993. **12**(10): p. 3799-808.

68. Boukhelifa, M., et al., *Palladin is a novel binding partner for Ena/VASP family members.* Cell Motil Cytoskeleton, 2004. **58**(1): p. 17-29.

69. Boukhelifa, M., et al., *A role for the cytoskeleton-associated protein palladin in neurite outgrowth.* Mol Biol Cell, 2001. **12**(9): p. 2721-9.

70. Ronty, M.J., et al., *Isoform-specific regulation of the actin-organizing protein palladin during TGF-beta1-induced myofibroblast differentiation.* J Invest Dermatol, 2006. **126**(11): p. 2387-96.

71. Goicoechea, S.M., et al., *Palladin contributes to invasive motility in human breast cancer cells.* Oncogene, 2009. **28**(4): p. 587-98.

72. Gupta, V., et al., *Elevated expression of stromal palladin predicts poor clinical outcome in renal cell carcinoma.* PLoS One, 2011. **6**(6): p. e21494.

73. Brentnall, T.A., et al., *Arousal of cancer-associated stroma: overexpression of palladin activates fibroblasts to promote tumor invasion.* PLoS One, 2012. **7**(1): p. e30219.

74. Chin, Y.R. and A. Toker, *The actin-bundling protein palladin is an Akt1-specific substrate that regulates breast cancer cell migration.* Mol Cell, 2010. **38**(3): p. 333-44.

75. Chin, Y.R. and A. Toker, *Akt2 regulates expression of the actin-bundling protein palladin.* FEBS Lett, 2010. **584**(23): p. 4769-74.

76. Chin, Y.R. and A. Toker, *Function of Akt/PKB signaling to cell motility, invasion and the tumor stroma in cancer.* Cell Signal, 2009. **21**(4): p. 470-6.

77. Miller, T.W., et al., *Mutations in the phosphatidylinositol 3-kinase pathway: role in tumor progression and therapeutic implications in breast cancer.* Breast Cancer Res, 2011. **13**(6): p. 224.

78. Ruddon, R.W., *Cancer Biology*. Fourth ed2007, New York, NY: Oxford University Press.

79. Franke, T.F., et al., *The protein kinase encoded by the Akt proto-oncogene is a target of the PDGF-activated phosphatidylinositol 3-kinase.* Cell, 1995. **81**(5): p. 727-36.

80. Irie, H.Y., et al., *Distinct roles of Akt1 and Akt2 in regulating cell migration and epithelial-mesenchymal transition.* J Cell Biol, 2005. **171**(6): p. 1023-34.

81. Dillon, R.L., D.E. White, and W.J. Muller, *The phosphatidyl inositol 3-kinase signaling network: implications for human breast cancer.* Oncogene, 2007. **26**(9): p. 1338-45.

82. Chin, Y.R. and A. Toker, *Akt isoform-specific signaling in breast cancer: uncovering an anti-migratory role for palladin.* Cell Adh Migr, 2011. **5**(3): p. 211-4.

83. Janji, B., et al., *Phosphorylation on Ser5 increases the F-actin-binding activity of L-plastin and promotes its targeting to sites of actin assembly in cells.* J Cell Sci, 2006. **119**(Pt 9): p. 1947-60.

84. Gautreau, A., D. Louvard, and M. Arpin, *Morphogenic Effects of Ezrin Require a Phosphorylation-Induced Transition from Oligomers to Monomers at the Plasma Membrane.* J Cell Biol, 2000. **150**(1): p. 193-204.

85. Clarke, D.M., et al., *Phosphorylation of actopaxin regulates cell spreading and migration.* J Cell Biol, 2004. **166**(6): p. 901-912.

86. Spudich, J.A. and S. Watt, *The regulation of rabbit skeletal muscle contraction. I. Biochemical studies of the interaction of the tropomyosin-troponin complex with actin and the proteolytic fragments of myosin.* J Biol Chem, 1971. **246**(15): p. 4866-71.

87. Schneider, C.A., W.S. Rasband, and K.W. Eliceiri, *NIH Image to ImageJ: 25 years of image analysis.* Nat Methods, 2012. **9**(7): p. 671-5.

88. Hiromasa, Y., L. Hu, and T.E. Roche, *Ligand-induced effects on pyruvate dehydrogenase kinase isoform 2.* J Biol Chem, 2006. **281**(18): p. 12568-79.

89. Stafford, W. *Reversible Associations in Structural and Molecular Biology*. 2013 [cited 2013 March 15th 2013].

90. Vardar, D., et al., *Villin-type headpiece domains show a wide range of F-actin-binding affinities.* Cell Motil Cytoskeleton, 2002. **52**(1): p. 9-21.

91. Wen, K.K., P.A. Rubenstein, and K.A. DeMali, *Vinculin nucleates actin polymerization and modifies actin filament structure.* J Biol Chem, 2009. **284**(44): p. 30463-73.

92. Johnson, R.P. and S.W. Craig, *Actin activates a cryptic dimerization potential of the vinculin tail domain.* J Biol Chem, 2000. **275**(1): p. 95-105.

93. Weith, A., et al., *Unique single molecule binding of cardiac myosin binding protein-C to actin and phosphorylation-dependent inhibition of actomyosin motility requires 17 amino acids of the motif domain.* J Mol Cell Cardiol, 2012. **52**(1): p. 219-27.

94. Anand, G.S., et al., *Evidence for phosphorylation-dependent conformational changes in methylesterase CheB.* Protein Sci, 2000. **9**(5): p. 898-906.

95. Kenney, L.J., M.D. Bauer, and T.J. Silhavy, *Phosphorylation-dependent conformational changes in OmpR, an osmoregulatory DNA-binding protein of Escherichia coli.* Proc Natl Acad Sci U S A, 1995. **92**(19): p. 8866-70.

96. Panayotou, G., et al., *Interaction of the p85 subunit of PI 3-kinase and its N-terminal SH2 domain with a PDGF receptor phosphorylation site: structural features and analysis of conformational changes.* EMBO J, 1992. **11**(12): p. 4261-72.

97. Artym, V.V., et al., *Dynamic interactions of cortactin and membrane type 1 matrix metalloproteinase at invadopodia: defining the stages of invadopodia formation and function.* Cancer Res, 2006. **66**(6): p. 3034-43.

98. Albiges-Rizo, C., et al., *Actin machinery and mechanosensitivity in invadopodia, podosomes and focal adhesions.* J Cell Sci, 2009. **122**(Pt 17): p. 3037-49.